

Accuracy-robustness trade-off via spiking neural network gradient sparsity trail

Luu Trong Nhan^{1, 3}, Luu Trung Duong², Pham Ngoc Nam³, and Truong Cong Thang⁴

¹College of Information and Communication Technology, Can Tho University, Vietnam

²Center of Digital Transformation and Communication, Can Tho University, Vietnam

³College of Engineering and Computer Science, VinUniversity, Hanoi, Vietnam

⁴Department of Computer Science and Engineering, The University of Aizu, Japan

Corresponding author:

Luu Trong Nhan

Email address: luutn@ctu.edu.vn

ABSTRACT

Spiking Neural Networks (SNNs) have attracted growing interest in both computational neuroscience and artificial intelligence, primarily due to their inherent energy efficiency and compact memory footprint. However, achieving adversarial robustness in SNNs, (particularly for vision-related tasks) remains a nascent and underexplored challenge. Recent studies have proposed leveraging sparse gradients as a form of regularization to enhance robustness against adversarial perturbations. In this work, we present a surprising finding: under specific architectural configurations, SNNs exhibit natural gradient sparsity and can achieve state-of-the-art adversarial defense performance without the need for any explicit regularization. Further analysis reveals a trade-off between robustness and generalization: while sparse gradients contribute to improved adversarial resilience, they can impair the model's ability to generalize; conversely, denser gradients support better generalization but increase vulnerability to attacks. Our findings offer new insights into the dual role of gradient sparsity in SNN training.

1 INTRODUCTION

Recent decades have witnessed remarkable progress in the domain of artificial intelligence (AI), primarily fueled by the evolution of deep learning techniques (Wani et al., 2020). Nevertheless, conventional artificial neural networks (ANNs) often struggle to accurately replicate the complex and dynamic characteristics inherent in biological neural systems (Nguyen et al., 2021). In response to this limitation, spiking neural networks (SNNs) have gained attention as a biologically inspired alternative, exploiting the temporal dynamics of neuronal signaling to better reflect the functioning of the human brain.

SNNs communicate using discrete spike events, emulating the asynchronous and event-driven nature of biological neural communication (Auge et al., 2021). This spike-based mechanism not only improves the biological realism of computational models but also introduces benefits such as enhanced energy efficiency and suitability for neuromorphic hardware implementations (Blouw et al., 2019). The sparsity and temporally precise signaling intrinsic to SNNs make them ideal candidates for designing power-efficient systems capable of real-time processing (Rajendran et al., 2019). Despite their advantages, SNNs presented notable difficulties, particularly in terms of training and optimization. The non-differentiable nature of spike-based activity renders traditional backpropagation techniques unsuitable (Nunes et al., 2022). To overcome these obstacles, researchers have proposed alternative training paradigms, including spike-timing-dependent plasticity (STDP) (Srinivasan et al., 2017; Liu et al., 2021) and surrogate gradient methods (Neftci et al., 2019; Eshraghian et al., 2023; Fang et al., 2021a), which facilitate the learning process in spiking networks.

Robustness remains a fundamental challenge AI, particularly within safety-critical domains such as autonomous driving, where adversarial attacks—small, human-imperceptible input perturbations—can induce high-confidence misclassifications (Szegedy et al., 2013; Goodfellow et al., 2014). Despite

substantial progress in defensive methodologies (Ross et al., 2017), neural models continue to exhibit vulnerability across diverse architectures, even when trained for the same task (Madry et al., 2017).

Distinct from ANNs, SNNs process spike-based temporal signals, introducing unique considerations for adversarial vulnerability (Sharmin et al., 2020). Prior studies have suggested that SNNs exhibit inherent robustness under rate-based conversion schemes (Sharmin et al., 2020; Kundu et al., 2021) and can be further regularized adversarially when directly coded inputs are employed (Ding et al., 2022; Liu et al., 2024). Nevertheless, the adversarial properties of SNNs under temporally coded inputs remain relatively underexplored.

Another crucial aspect of adversarial robustness lies in the intrinsic trade-off between accuracy and resistance to perturbation (Tsipras et al., 2018). While the theoretical underpinnings of this trade-off have been extensively studied in the context of ANNs (Tsipras et al., 2018), a systematic investigation of similar phenomena in SNNs has not yet been presented.

In this work, we investigate the role of *gradient sparsity* in SNNs and its influence on the robustness–generalization trade-off, particularly in the context of event-based inputs under adversarial perturbations. Through comprehensive empirical evaluation and theoretical analysis, we report the following key findings:

- **Natural robustness under temporal spike-based backpropagation:** Similar to SNNs with rate-based conversion (Sharmin et al., 2019, 2020), temporally coded SNNs (Kim et al., 2018) demonstrate an inherent degree of natural robustness under surrogate training context, achieving state-of-the-art (SOTA) adversarial resistance without explicit defensive regularization (Ding et al., 2022) or auxiliary mechanisms (Kundu et al., 2021; Sharmin et al., 2020).
- **Trade-off via gradient sparsity:** Similarly to ANN (Tsipras et al., 2018), this natural robustness incurs a reduction in clean (undefended) accuracy. Through empirically architectural manipulation and theoretical derivation, we show that the shared computational pathway between input and weight gradients induces gradient sparsity, which propagates to both. Consequently, this sparsity suppresses model expressivity and weakens adversarial gradients, thereby dampening both clean performance and attack efficacy. Conversely, intentionally increasing internal gradient density improves clean generalization but simultaneously diminishes robustness to adversarial perturbations.

To the best of our knowledge, this is the first work to systematically identify and characterize the dual role of gradient sparsity in governing the robustness–accuracy trade-off within spiking neural networks.

2 RELATED WORKS

2.1 Spiking Neural Networks

SNNs represent a biologically inspired extension of traditional ANNs, offering a fundamentally distinct computational framework. In contrast to ANNs, which utilize continuous-valued activations and gradient-based learning algorithms such as backpropagation (Rumelhart et al., 1986; Shrestha and Orchard, 2018), SNNs encode and transmit information through discrete spike events (Maass, 1997). This event-driven mechanism supports sparse and energy-efficient computation, making SNNs particularly well-suited for deployment on neuromorphic hardware (Merolla et al., 2014). While most conventional ANN architectures operate on dense, floating-point representations, SNNs emulate the asynchronous and temporally precise signaling of biological neurons (Gerstner and Kistler, 2002). Additionally, SNNs inherently process temporal data and can leverage learning rules like STDP for unsupervised training (Lee et al., 2018). However, the discontinuous nature of spikes presents significant challenges for optimization, often requiring alternative training strategies such as surrogate gradient methods (Neftci et al., 2019), hybrid model training (Luu et al., 2025) or indirect approaches like ANN-to-SNN conversion (Rueckauer et al., 2017). As a result, SNNs offer a promising direction for energy-efficient and biologically plausible computation, while also posing distinct challenges in terms of training and network design.

Various surrogate gradient functions have been proposed (Fang et al., 2023, 2021a; Zenke and Ganguli, 2018; Esser et al., 2015; Zenke and Vogels, 2021), each with different trade-offs in terms of biological fidelity, computational efficiency, and training stability. These approximations enable effective error propagation through spiking layers, making it possible to train deep SNN architectures for complex image processing tasks (Fang et al., 2021a; Lee et al., 2020; Shrestha and Orchard, 2018). Together,

these developments have contributed to bridging the performance gap between SNNs and their ANN counterparts, while maintaining the unique advantages of spiking computation.

2.2 Adversarial Robustness In Artificial Neural Network

ANNs can be easily deceived into producing incorrect outputs on inputs that have been subtly altered in ways imperceptible to humans (Szegedy et al., 2013). While many adversarial-example generation methods (usually referred to as “adversarial attacks”) rely on white-box access to model parameters, recent work has demonstrated that even black-box models can be compromised in practice—largely owing to the transferability property of adversarial examples, whereby inputs crafted to mislead one model often generalize to other models trained on the same data (Papernot et al., 2017). In the context of image recognition, adversarial perturbations can be crafted to remain effective across different scales and viewing angles (Athalye et al., 2018b), posing a significant challenge to deploying deep learning in safety-critical applications such as autonomous vehicles.

Despite a surge of research into adversarial defenses, many proposed methods fail to withstand transferred attacks (Tramèr et al., 2017b). For instance, “feature squeezing” (Xu et al., 2017) sidesteps robust classification by simply detecting and discarding suspected adversarial inputs rather than correctly classifying them. The most straightforward defense-adversarial training—augments the training set with a mixture of clean and adversarially-perturbed examples (Kurakin et al., 2016). However, Tramèr et al. (2017a) showed that adversarial training can be undermined by randomizing perturbations or borrowing perturbations generated from different models, although employing model ensembles offers some mitigation.

Beyond robustness, practitioners are often troubled by the opacity of DNN predictions. This lack of interpretability is especially problematic in domains prone to algorithmic bias (Flores et al., 2016) or in medical settings where discrepancies between training and deployment contexts can introduce safety hazards (Caruana et al., 2015). To address this, many methods aim to explain individual DNN decisions via interpretable local surrogate models—commonly linear approximations that capture the network’s behavior under small input perturbations (Ribeiro et al., 2016). A straightforward choice is to use the model’s input gradient, which provides a first-order Taylor approximation of how outputs change in response to input variations (Baehrens et al., 2010). However, for image classification, raw input gradients are often noisy and difficult to interpret. Consequently, techniques such as Integrated Gradients (Sundararajan et al., 2016) and SmoothGrad (Smilkov et al., 2017) have been developed to produce smoother, more visually coherent saliency maps by aggregating gradient information across multiple perturbed copies of the input.

2.3 Adversarial Robustness in Spiking Neural Network

While adversarial attacks have been extensively investigated in ANNs, their study in SNNs remains comparatively limited, with research in this domain still at an early stage. For image-based attacks, Sharmin et al. (2019) examined the vulnerabilities of SNNs and their ANN counterparts under both white-box and black-box conditions, focusing on single-step and multi-step FGSM attacks. To circumvent the non-differentiable nature of spiking neurons, the authors reformulated the attack process through an ANN-based surrogate model that replicated the SNN’s architecture and parameters. Adversarial examples crafted via this surrogate approach were found to be substantially more effective against SNNs than ANNs.

Building on this, Sharmin et al. (2020) introduced an approximate surrogate gradient method to address the discontinuities in the gradients of LIF and IF neurons. Liang et al. (2021) further identified key challenges in attacking SNNs, such as the incompatibility between spiking inputs and continuous gradients and the tendency for gradient vanishing. To mitigate these issues, they proposed the Gradient-to-Spike (G2S) converter, which transforms continuous gradients into ternary spike-compatible gradients, and the Restricted Spike Flipper (RSF), which alleviates vanishing gradient effects. These contributions enabled the development of a more principled gradient-based adversarial framework tailored to SNNs, underscoring the distinct nature of their adversarial behavior.

In parallel, Marchisio et al. (2020) proposed a greedy black-box algorithm for generating adversarial examples using both normally and uniformly distributed random noise. More recently, Bu et al. (2023) presented the Rate Gradient Approximation (RGA) attack, which demonstrates lower sensitivity to neuronal hyperparameters and improved consistency across neuron models and encoding schemes compared to prior approaches such as Spike-Time-Dependent Backpropagation (STBP). Lin et al. (2022a) advanced

this line of work through the Spiking Feature Transferable Attack (SFTA), enhancing transferability by suppressing robust positive features, while Lin et al. (2022b) introduced the Spike Probabilistic Attack (SPA), leveraging Poisson-based perturbations to achieve efficient and uniformly distributed adversarial noise generation.

3 ADVERSARIAL ATTACKS

In this section, we establish the notation used throughout while briefly outline the standard adversarial attack mechanisms that serve as baselines for comparison, which applies to any differentiable classifier denoted by $f_\theta(X)$, where θ represents the model parameters. The model produces prediction outputs $\hat{y} \in \mathbb{R}^{N \times K}$ for input data $X \in \mathbb{R}^{N \times D}$, with N samples of dimensionality D , each classified into one of K categories. These predictions correspond to class probabilities for each input instance.

Training such models involves optimizing the parameter set θ^* to minimize the divergence between the predicted outputs \hat{y} and the ground truth labels $y \in \mathbb{R}^{N \times K}$ (represented in one-hot encoding). This is typically achieved by minimizing the overall cross-entropy loss (Ross and Doshi-Velez, 2018):

$$\begin{aligned}\theta^* &= \arg \min_{\theta} \sum_{n=1}^N \sum_{k=1}^K -y_{nk} \log f_\theta(X_n)_k \\ &= \arg \min_{\theta} H(y, \hat{y})\end{aligned}\tag{1}$$

where H denotes the total cross-entropy between the true and predicted distributions.

3.1 Fast Gradient Sign Method (FGSM)

Introduced by Goodfellow et al. (2014), this approach perturbs input samples in the direction of the gradient sign of the loss with respect to the inputs. The perturbed adversarial examples are given by:

$$X_{\text{FGSM}} = X + \epsilon \cdot \text{sign}(\nabla_x H(y, \hat{y})),\tag{2}$$

where ϵ controls the magnitude of the perturbation. Although small in scale, these modifications can substantially degrade model performance while remaining imperceptible to human observers. Kurakin et al. (2018) extended this method by applying it multiple times with smaller step sizes. This iterative variant follows the gradient path more accurately, resulting in stronger adversarial examples that require less overall distortion.

3.2 Projected Gradient Descent (PGD)

Building upon the FGSM framework, the PGD attack (introduced by Madry et al. (2017)) is considered one of the most potent first-order adversaries. It generates adversarial examples by iteratively applying small perturbations in the direction of the gradient sign of the loss with respect to the input, while projecting the perturbed input back onto the ℓ_∞ ball of radius ϵ centered around the original input. Formally, each update step is given by:

$$X^{t+1} = \Pi_{\mathcal{B}_\epsilon(X)}(X^t + \alpha \cdot \text{sign}(\nabla_x H(y, \hat{y}))),\tag{3}$$

where $\Pi_{\mathcal{B}_\epsilon(X)}(\cdot)$ denotes the projection operator onto the ℓ_∞ ball $\mathcal{B}_\epsilon(X)$, α is the step size, and t is the iteration index. By repeating this process for multiple steps, PGD generates adversarial examples that are more effective at deceiving neural networks, while still remaining within the specified perturbation bound. This iterative process significantly enhances attack strength compared to single-step methods like FGSM.

4 EVALUATION AND ANALYSIS

4.1 Overall settings

For undefended benchmarking, we employed SEW-ResNet (Fang et al., 2021a) and Spiking-ResNet (Hu et al., 2021) variants. Model implementation and experimental procedures leveraged PyTorch (Paszke et al., 2019) and SpikingJelly (Fang et al., 2023).

For preprocessing, we performed image normalization within the range of [0, 1] and horizontal random flip during training as augmentation method (Wang and Perez, 2017) for better generalization.

Optimization was facilitated by applying Backward Pass Through Time (BPTT) (Ding et al., 2022; Fang et al., 2021b) with surrogate gradient (Fang et al., 2021a) to all Integrate-and-Fire (IF) neurons, utilizing the arctan surrogate function (Fang et al., 2021a; Eshraghian et al., 2023). Its derivative, $\partial\Theta/\partial x$, for the Heaviside function $\Theta(x, V_{th})$ with potential voltage V_{th} and input x during backpropagation is defined as:

$$\Theta(x, V_{th}) = \begin{cases} 1 & \text{if } x - V_{th} \geq 0 \\ 0 & \text{otherwise} \end{cases} \quad (4)$$

$$\frac{\partial\Theta}{\partial x} = \frac{\alpha}{2 \left(1 + \left(\frac{\pi}{2}\alpha x\right)^2\right)} \quad \text{where } \alpha = 2$$

For spike encoding, we adopted the well-established *phase coding* (Kim et al., 2018) with a time step size of $T = 10$, spike weight $\omega(t)$ where $t \in T$ is given by:

$$\omega(t) = 2^{-(1+\text{mod}(t-1, K))}.$$

Consistent with prior work in ANN and SNN optimization (Luu et al., 2023, 2024a,b,c), cross-entropy loss (mentioned in Equation 1) along with the Adam algorithm (Kingma and Ba, 2014) was used for optimization. A learning rate of $lr = 1 \times 10^{-3}$ and parameters $\beta = (0.9, 0.999)$ were applied for optimizer across all evaluated datasets. All training was conducted with a batch size of 16 images for 100 epochs on an NVIDIA RTX 3090 GPU. We also use deterministic random seeding (Picard, 2021) to ensure reproducibility and avoid stochastic gradient problem (Athalye et al., 2018a). To evaluate the comparative performance of our model in image classification tasks, we utilize *Accuracy*—a widely adopted metric that quantifies how well a model predicts the correct labels. Specifically, accuracy represents the ratio of correctly predicted labels \hat{y}_i matching the true labels y_i across a dataset of N instances, and is formally defined as:

$$\text{Accuracy} = \frac{1}{N} \sum_{i=1}^N \mathbb{1}(\hat{y}_i = y_i)$$

Here, $\mathbb{1}(\cdot)$ denotes the indicator function, which yields 1 if the argument is true and 0 otherwise.

4.2 Natural adversarial robustness of SNN over temporal-coded backpropagation

We benchmark our selected models on CIFAR10, CIFAR100 (Alex, 2009) and CIFAR10-DVS (Li et al., 2017) against several SOTA methods aimed at enhancing the adversarial robustness of spiking neural networks. Specifically, we compare our undefended SNN variants with input discretization (Sharmin et al., 2020), Hire-SNN (Kundu et al., 2021), and SNN-RAT (Ding et al., 2022), all of which have demonstrated notable improvements under adversarial settings. The evaluations will focus on standard attack methods such as FGSM and PGD and all models will be benchmarked using fixed settings for adversarial attacks. Specifically, $\epsilon = 8/255$ will be used for both FGSM and PGD, with PGD further configured with $\alpha = 0.01$ and $t = 7$, consistent with previous researches (Ding et al., 2022). A visualization of the perturbated images are presented in Figure 1.

As presented in Table 1, all SEW-ResNet variants exhibit SOTA performance against PGD attacks, achieving up to 16.03% accuracy—an improvement of 4.72% over the previous best method (SNN-RAT WRN-16). For FGSM attacks, SEW-ResNet50 yields a competitive 21.27% accuracy, which is only 4.59% below SNN-RAT and nearly equivalent to the performance of Hire-SNN, leading us to suspect that the benchmarking result was affected by obfuscated gradient (Athalye et al., 2018a). In contrast, Spiking-ResNet variants without any defense mechanism do not exhibit similar resilience as deeper residual blocks being constructed, therefore we would only continue benchmarking with SEW-ResNet variants. From Table 2, we can see that this behavior not only consistent on multiple dataset, SEW-ResNet was able to outperform almost all mentioned adversarial defense mechanism:

- SEW-ResNet50 with a 0.31% gap on FGSM and 17.84% gap on PGD (compare with SNN-RAT WRN-16 on CIFAR10),
- SEW-ResNet50 with a 4.72% gap on PGD (compare with SNN-RAT WRN-16 on CIFAR100),

Table 1. Comparison of CIFAR-100 (Alex, 2009) validation accuracy of undefended SNN variants with various SNN adversarial defense methods. Best performance per attack are denoted in bold. The upper section showcases the accuracy of existing SOTA defend methods, while the lower section details the performance of undefended SEW-ResNet and Spiking-ResNet variants. Notably, undefended SEW-ResNet achieve SOTA performance against PGD attacks and reasonable performance against FGSM attacks.

SNN variants	Validation accuracy per attack (%)		
	FGSM	PGD	Clean
Input discretization (Sharmin et al., 2020)	15.50	6.30	64.40
Hire-SNN (Kundu et al., 2021)	22.00	7.50	65.10
Vanilla VGG-11 (Ding et al., 2022)	5.30	0.02	73.33
SNN-RAT VGG-11 (Ding et al., 2022)	25.86	10.38	70.89
SNN-RAT WRN-16 (Ding et al., 2022)	28.08	11.31	69.32
SEW-ResNet18 (Fang et al., 2021a)	20.81	13.47	42.19
SEW-ResNet34 (Fang et al., 2021a)	19.91	13.25	41.81
SEW-ResNet50 (Fang et al., 2021a)	21.27	16.03	38.91
Spiking-ResNet18 (Hu et al., 2021)	13.36	11.15	23.23
Spiking-ResNet34 (Hu et al., 2021)	2.43	1.64	21.20
Spiking-ResNet50 (Hu et al., 2021)	3.32	2.44	20.56

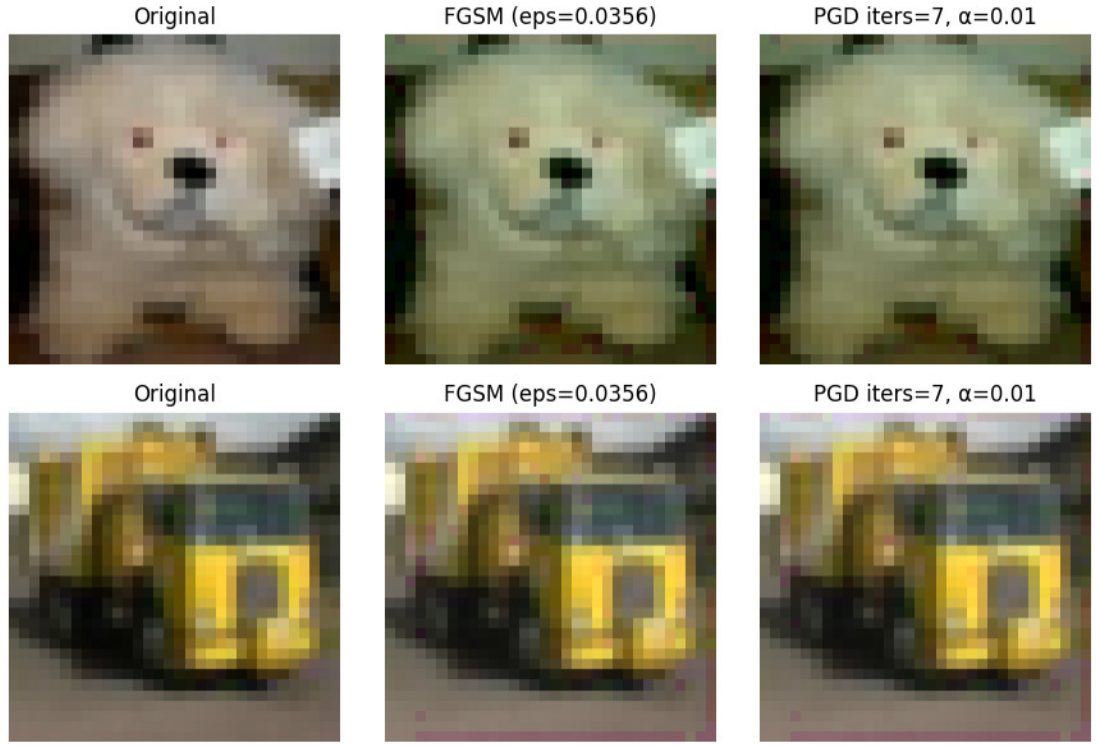


Figure 1. Example illustration of perturbated images from CIFAR-10 with FGSM and PGD over a network.

- SEW-ResNet34 with a 8.87% gap on FGSM (compare with SNN-RAT WRN-16 on CIFAR10-DVS) and SEW-ResNet50 with a 3.32% gap on PGD (compare with SNN-RAT VGG-11 on CIFAR10-DVS).

Table 2. Comparison of validation accuracy of undefended SEW-ResNet variants with various SNN adversarial defense methods on multiple vision datasets. Best performance per attack on each dataset are denoted in bold. Results are consistent even with different datasets.

Datasets	SNN variants	Validation accuracy per attack (%)		
		FGSM	PGD	Clean
CIFAR10	SNN-RAT VGG-11 (Ding et al., 2022)	45.23	21.16	90.74
	SNN-RAT WRN-16 (Ding et al., 2022)	50.78	22.71	92.69
	SEW-ResNet18 (Fang et al., 2021a)	46.99	34.33	73.78
	SEW-ResNet34 (Fang et al., 2021a)	49.20	36.98	74.16
	SEW-ResNet50 (Fang et al., 2021a)	51.09	40.55	73.34
CIFAR100	SNN-RAT VGG-11 (Ding et al., 2022)	25.86	10.38	70.89
	SNN-RAT WRN-16 (Ding et al., 2022)	28.08	11.31	69.32
	SEW-ResNet18 (Fang et al., 2021a)	20.81	13.47	42.19
	SEW-ResNet34 (Fang et al., 2021a)	19.91	13.25	41.81
	SEW-ResNet50 (Fang et al., 2021a)	21.27	16.03	38.91
CIFAR10-DVS	SNN-RAT VGG-11 (Ding et al., 2022)	36.22	19.02	71.77
	SNN-RAT WRN-16 (Ding et al., 2022)	40.16	17.11	76.12
	SEW-ResNet18 (Fang et al., 2021a)	47.19	21.47	75.18
	SEW-ResNet34 (Fang et al., 2021a)	49.03	18.65	75.29
	SEW-ResNet50 (Fang et al., 2021a)	48.52	22.34	76.53

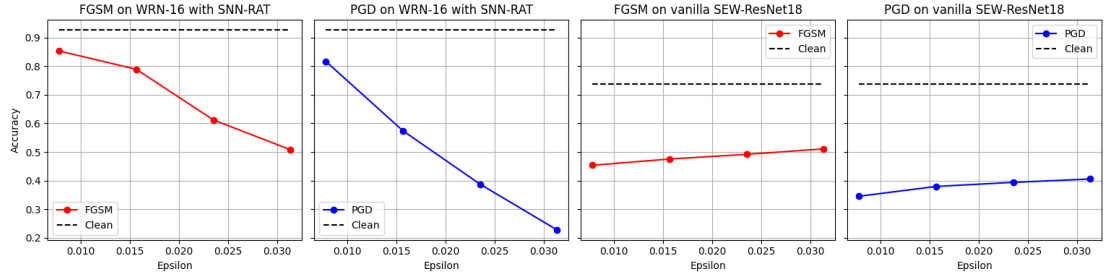


Figure 2. Effect of adversarial attacks over multiple perturbation magnitude ϵ between defended WideResNet16 and vanilla SEW-ResNet18.

We further investigate the adversarial robustness of the benchmarked models across varying perturbation magnitudes, specifically at $\epsilon \in \{2, 4, 6, 8\}/255$. As illustrated in Figure 2, the accuracy of the regularized WideResNet-16 progressively decreases as the input perturbation increases, with performance reductions of approximately 35% under FGSM and 70% under PGD attacks. In contrast, SEW-ResNet exhibits relatively higher vulnerability to smaller perturbations, showing performance degradations of about 25% under FGSM and 35% under PGD, which is consistent with behavior validated by prior work regarding the effect of small scale perturbation on SNN (Liu et al., 2024).

4.3 Gradient analysis and theoretical explanation

4.3.1 Gradient analysis

As demonstrated in the benchmarking results presented in Section 4.2, we observe that undefended SEW-ResNet exhibit a notable degree of adversarial robustness, achieving performance comparable to SOTA defense methods but Spiking-ResNet does not exhibit the same behavior. This raises some fundamental questions:

- *Why do SNNs demonstrate such inherent robustness in the absence of explicit defense mechanisms?*

We hypothesize that this phenomenon arises from the inherent sparsity of input gradients in SEW-ResNet, which in turn reduces the efficacy of adversarial perturbations while also make small scale perturbation to yield stronger effect. Supporting this hypothesis, prior work has shown that the strength

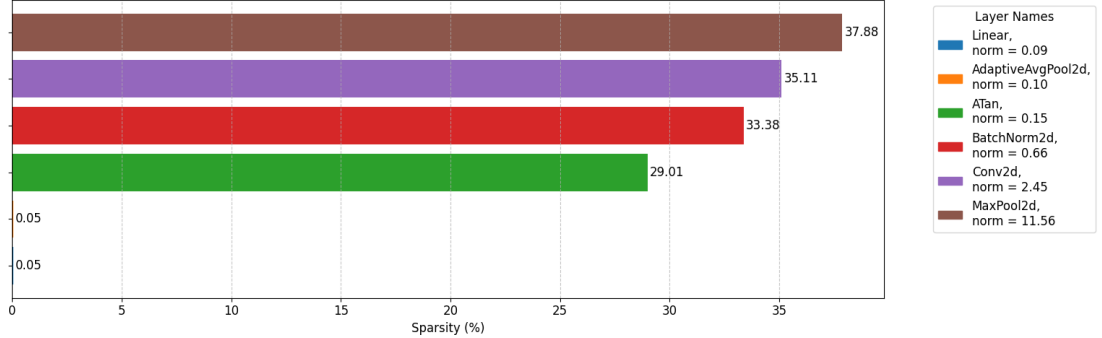


Figure 3. Inspection of average input gradient sparsity and input gradient norm across all employed operations within SEW-ResNet18. Gradient was clearly defined and high sparsity mostly occurs in operations of SEW residual blocks.

of adversarial attacks can be upper bounded by the sparsity of the input gradient. Specifically, Liu et al. (2024) established the following theoretical bound:

Theorem 4.1 (Liu et al. (2024)). *Suppose f is a differentiable SNN by surrogate gradients, and ϵ is the magnitude of an attack, assumed to be small enough. Given an input image \mathbf{x} with corresponding label y , the ratio of adversarial vulnerability $\rho_{adv}(f, \mathbf{x}, \epsilon, \ell_\infty)$ and random vulnerability $\rho_{rand}(f, \mathbf{x}, \epsilon, \ell_\infty)$ is upper bounded by the density of input gradient $\nabla_{\mathbf{x}} f_y$ as:*

$$3 \leq \frac{\rho_{adv}(f, \mathbf{x}, \epsilon, \ell_\infty)}{\rho_{rand}(f, \mathbf{x}, \epsilon, \ell_\infty)} \leq 3 \|\nabla_{\mathbf{x}} f_y(\mathbf{x})\|_0. \quad (5)$$

where $\rho_{adv}(f, \mathbf{x}, \epsilon, \ell_\infty)$ scale linearly with non-zeros entries (L_0 norm) of input gradient $\|\nabla_{\mathbf{x}} f_y(\mathbf{x})\|_0$.

Proof for this theorem is denoted in Appendix A.

To validate this explanation in light of the theorem, we conduct an empirical analysis of the input gradient patterns for SEW-ResNet models under adversarial perturbations. Specifically, we compute the average percentage of non-zero entries in the input gradients (as shown in Figure 3). Additionally, we measure the gradient norm to ensure that the sparsity is not a byproduct of shattered gradients, following the recommendations from Athalye et al. (2018a).

While gradient was clearly defined as norm was calculable, gradient sparsity emerges predominantly within residual blocks from 29.01% in IF neurons surrogate gradient to 37.88% in max pooling gradient, particularly in components such as convolutional layers, batch normalization, max pooling, and arctan surrogate gradients of IF neurons. This sparsity may serve as a natural regularization mechanism, assisting in gradient-based attacks mitigation and contributing to the enhanced robustness observed in our experiments.

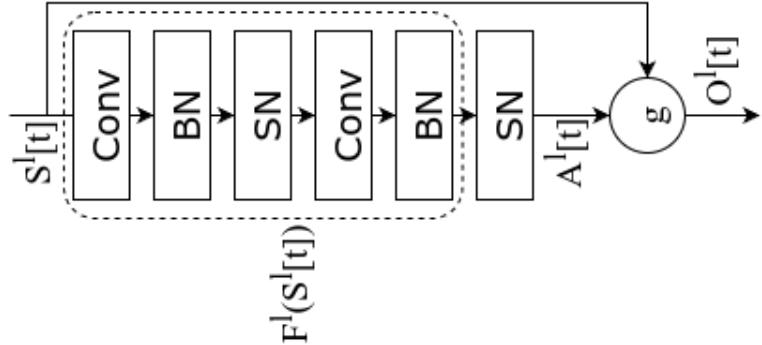


Figure 4. Architecture of SEW residual block proposed by Fang et al. (2021a)

$$\begin{aligned}
\frac{\partial \mathbf{Conv}(x, \mathbf{w})}{\partial x} &= \mathbf{Conv}^\top \left(\frac{\partial \mathcal{L}}{\partial y}, \mathbf{w} \right), \\
\frac{\partial \mathbf{BN}(y_{i,c})}{\partial x_{i,c}} &= \frac{\gamma_c}{\sqrt{\sigma_c^2 + \varepsilon}} \left[\delta_{i,c} - \sum_j^m \frac{\delta_{j,c}}{m} - \frac{\hat{x}_{i,c}}{m} \sum_j^m \delta_{j,c} \cdot \hat{x}_{j,c} \right], \\
\delta_{i,c} &= \frac{\partial \mathcal{L}}{\partial y_{i,c}} \\
\hat{x}_{i,c} &= \frac{x_{i,c} - \mu_c}{\sqrt{\sigma_c^2 + \varepsilon}}, \quad y_{i,c} = \gamma_c \hat{x}_{i,c} + \beta_c \\
\mu_c &= \frac{1}{m} \sum_{i=1}^m x_{i,c}, \quad \sigma_c^2 = \frac{1}{m} \sum_{i=1}^m (x_{i,c} - \mu_c)^2 \\
\frac{\partial \mathbf{MaxPool}(x)}{\partial x_{i,j}} &= \begin{cases} \frac{\partial \mathcal{L}}{\partial y_{p,q}} & \text{if } x_{i,j} = \max_{(m,n) \in \mathcal{R}_{p,q}} x_{m,n} \\ 0 & \text{otherwise} \end{cases} \\
\frac{\partial \Theta}{\partial x} &= \frac{\alpha}{2 \left(1 + \left(\frac{\pi}{2} \alpha x \right)^2 \right)} \quad \text{where } \alpha = 2
\end{aligned} \tag{6}$$

Upon further analysis, we identified two distinct types of gradient sparsity emerging from these operations, which we categorize as:

- *Architectural sparsity* where input gradient sparsity occurred mostly due to intentional architectural choice.
- *Natural sparsity* where input gradient sparsity occurred due to the nature of spike signal instead of model design influence.

To quantify these sources, we analyze the gradient expressions of each component within the spike-based element-wise residual blocks. As seen in Equation 6, convolution **Conv**, batch normalization **BN**, and surrogate gradient components Θ are all dependent on input and intermediate values. However, max pooling **MaxPool** introduces a structural bottleneck where gradients are non-zero only at the maximum activation locations, and zero elsewhere. These null gradients can propagate through backward pass, create sparsity in earlier layers and is denoted as *architectural sparsity*. This effect is amplified in SEW-ResNet due to the high coupling nature of residual blocks (illustrated in Figure 4). Thus, replacing max pooling with a less sparse alternative could enhance gradient density. To evaluate this hypothesis, we replaced max pooling **MaxPool** operations with average pooling **AvgPool**, whose gradient is given by:

$$\frac{\partial \mathbf{AvgPool}}{\partial x_{i,j}} = \sum_{(p,q) : (i,j) \in \mathcal{R}_{p,q}} \frac{1}{|\mathcal{R}_{p,q}|} \cdot \frac{\partial \mathcal{L}}{\partial y_{p,q}} \tag{7}$$

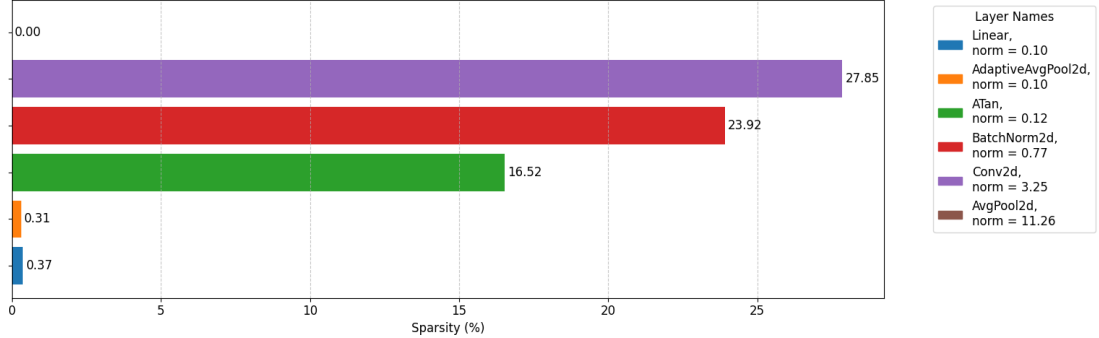


Figure 5. Inspection of average input gradient sparsity and input gradient norm across all employed operations within SEW-ResNet18 when employed with average pooling. Sparsity significantly reduced when compared with result in Figure 3.

Table 3. Comparison of CIFAR-100 and CIFAR-10 validation accuracy of undefended SEW-ResNet variants (Fang et al., 2021a) with average pooling. Best performance per attack on each dataset are denoted in bold. We employed similar attack settings as Table 1, accuracy reduction with respect to Table 2 is denoted in red and accuracy increment is denoted in green. There is a clear trade off in clean accuracy and adversarial robustness.

Datasets	SNN variants	Validation accuracy per attack (%)		
		FGSM	PGD	Clean
CIFAR-10	SEW-ResNet18	45.71 (↓1.28)	25.72 (↓8.61)	75.76 (↑1.98)
	SEW-ResNet34	48.72 (↓0.48)	29.82 (↓7.16)	76.17 (↑2.01)
	SEW-ResNet50	49.88 (↓1.21)	33.29 (↓7.26)	75.28 (↑1.94)
CIFAR-100	SEW-ResNet18	17.93 (↓2.88)	8.65 (↓4.82)	43.32 (↑1.13)
	SEW-ResNet34	20.07 (↓0.16)	10.37 (↓2.88)	44.58 (↑2.77)
	SEW-ResNet50	22.02 (↓0.74)	13.37 (↓2.66)	43.40 (↑4.49)
CIFAR10-DVS	SEW-ResNet18	46.27 (↓0.92)	13.94 (↓7.53)	77.77 (↑2.59)
	SEW-ResNet34	47.66 (↓1.37)	12.54 (↓6.11)	76.43 (↑1.14)
	SEW-ResNet50	47.01 (↓1.51)	14.30 (↓8.04)	78.35 (↑1.82)

This formulation distributes gradients evenly across all elements in the receptive field $\mathcal{R}_{p,q}$, effectively reducing the degree of gradient sparsity, allow it to have broader impact during gradient-based optimization. We then re-evaluate SEW-ResNet variants' performance under this setting and measure the resulting input gradient sparsity along with their adversarial robustness. The results are detailed in Figure 5 and Table 3.

From the results in Table 3, we observe that adversarial robustness of SEW-ResNet variants decrease when average pooling is employed in SEW-ResNet variants. Specifically, SEW-ResNet variants validation accuracy decrease under both FGSM and PGD attacks, with accuracy as low as 0.16% and 2.88% for SEW-ResNet34 on CIFAR-100 and as high as 1.28% and 8.61% for SEW-ResNet18 on CIFAR-10. Vice versa, models are able to improve generalization on clean validation, range from 1.13% (for SEW-ResNet18) to 4.49% (for SEW-ResNet50) on CIFAR-100.

As shown in Figure 5, input gradient sparsity is significantly reduced when average pooling is used in place of max pooling across all layers. Specifically, sparsity in the pooling layer is completely eliminated, leading to a 37.88% reduction compared to max pooling, while a spiking neuron layers exhibit sparsity as low as 16.52%. This observation is consistent with prior studies. For instance, Fang et al. (2021a) highlighted the importance of gradient magnitude in optimizing SNNs to enhance performance, while Luu et al. (2024b) addressed training challenges by introducing signal concatenation, effectively scaling the gradient norm to improve generalization. Complete elimination of sparsity is also theoretically unachievable due to the inherent sparse nature of spiking neurons in SNNs, typically modeled using the Heaviside function (as in Equation 4) and is referred to as *natural sparsity* within this context.

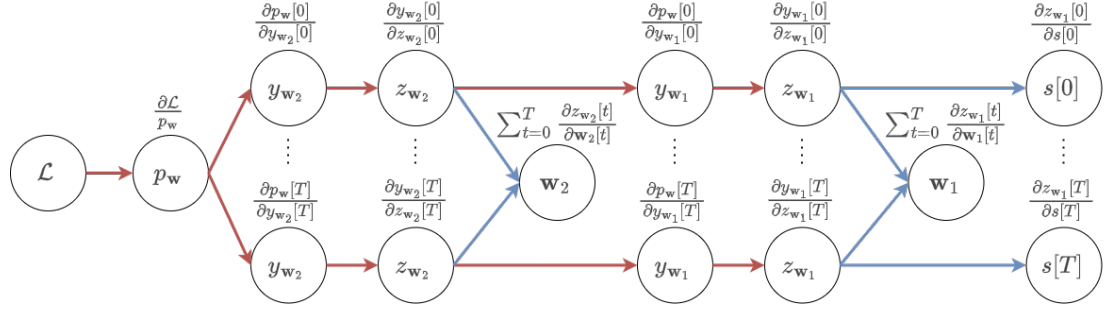


Figure 6. Backpropagation graph of Equation 8. Red arrow denoted shared gradient trails and blue denote variable specific gradient trail. Sparsity within shared gradient trail traverse to both input and optimizable parameters.

4.3.2 Theoretical explanation

Previous studies have demonstrated a strong relationship between the magnitude of weight gradients and model performance (Luu et al., 2024b; Fang et al., 2021a; Shalev-Shwartz et al., 2017). More specifically, Luu et al. (2024b) had proven the correlation between gradient scale and performance of a surrogate SNN model over gradient signal-to-noise-ratio (SNR) when scaling over temporal dimension T as follow:

Theorem 4.2 (Luu et al. (2024b)). *Assume that temporally-extended gradient $g_{\mathbf{w}}^{\text{extend}}(\mathbf{x})$ does not explode nor vanish, bounded as:*

$$G(\mathbf{w})^2 > \left\| \mathbb{E}_{\mathbf{x}} \left[g_{\mathbf{w}}^{\text{extend}}(\mathbf{x}) \right] \right\|_{\infty} > 0$$

for some scalar $G(\mathbf{w})$, where both gradient of baseline SNN $g_{\mathbf{w}}(\mathbf{x})$ and temporally extended SNN $g_{\mathbf{w}}^{\text{extend}}(\mathbf{x})$ converge toward a reasonable approximation of $h(\mathbf{x})$ and have similar distribution that satisfy:

$$\text{Cov} \left(h(\mathbf{x}), g_{\mathbf{w}}^{\text{extend}}(\mathbf{x}) \right) = 0, \quad \text{sign}(\mathbb{E}_{\mathbf{x}} [h(\mathbf{x})]) > 0, \quad h(\mathbf{x}) \cdot g_{\mathbf{w}}^{\text{extend}}(\mathbf{x}) \sim h(\mathbf{x}) \cdot g_{\mathbf{w}}(\mathbf{x}),$$

there exist:

$$\sup \left(\text{SNR} \left(\delta^{\text{extend}}(\mathbf{x}) \right) \right) \geq \sup \left(\text{SNR} \left(\delta(\mathbf{x}) \right) \right).$$

where:

$$\begin{aligned} \sup \left(\text{SNR} \left(\delta^{\text{extend}}(\mathbf{x}) \right) \right) &= \frac{\left\| \mathbb{E}_{\mathbf{x}} \left[\delta^{\text{extend}}(\mathbf{x}) \right] \right\|_{\infty}^2}{\mathbb{E}_{\mathbf{x}} \left\| \delta^{\text{extend}}(\mathbf{x}) - \mathbb{E}_{\mathbf{x}} \left[\delta^{\text{extend}}(\mathbf{x}) \right] \right\|_{\infty}^2}, \\ \sup \left(\text{SNR} \left(\delta(\mathbf{x}) \right) \right) &= \frac{\left\| \mathbb{E}_{\mathbf{x}} \left[\delta(\mathbf{x}) \right] \right\|_{\infty}^2}{\mathbb{E}_{\mathbf{x}} \left\| \delta(\mathbf{x}) - \mathbb{E}_{\mathbf{x}} \left[\delta(\mathbf{x}) \right] \right\|_{\infty}^2} \end{aligned}$$

Proof for this theorem can be found at Appendix B.

Building on this foundation, we aim to investigate how sparsity in the input gradients may suppress weight gradients during optimization, thereby influencing overall performance. To prove this statement, we consider the following theorem:

Theorem 4.3. *Given a multilayer SNN of the form:*

$$\begin{aligned} p_{\mathbf{w}}(s) &= \mathbb{E}_T [y_{\mathbf{w}_2}(y_{\mathbf{w}_1}(s[t]))] \quad \text{where } t \in T \\ y_{\mathbf{w}_1}(\mathbf{x}) &= \Theta(z_{\mathbf{w}_1}(\mathbf{x})), \quad z_{\mathbf{w}_1}(\mathbf{x}) = \mathbf{w}_1 \cdot \mathbf{x} \\ y_{\mathbf{w}_2}(\mathbf{x}) &= \Theta(z_{\mathbf{w}_2}(\mathbf{x})), \quad z_{\mathbf{w}_2}(\mathbf{x}) = \mathbf{w}_2 \cdot \mathbf{x} \end{aligned} \tag{8}$$

where $s[t] \in \{0,1\}^{T \times d}$ is the input signal, $\mathbf{w}_l \in \mathbb{R}^{d \times d}$ are the model parameter matrices at layer l and $\Theta(x, V_{th})$ is the hard-reset IF neurons with membrane potential V_{th} , defined as:

$$\Theta(s[t], V_{th}) = \begin{cases} 1 & \text{if } s[t] - V_{th} \geq 0 \\ 0 & \text{otherwise} \end{cases} \quad (9)$$

$$\frac{\partial \Theta}{\partial s[t]} = \frac{1}{1 + (\pi \cdot s[t])^2}$$

Then as a result, we would have the following:

- Any sparsity occur within the shared gradient chain will traverse back to both input gradient and weight gradient.
- Parameters that are placed closer to the initial input signal will shared a longer gradient chain, making sparsity in input gradient have a stronger correlation with parameter gradient.

Proof. The input gradient $\nabla_{s[t]} p_{\mathbf{w}}(s)$ of signal $s[t]$ at timestep t can be quantified as:

$$\begin{aligned} \nabla_{s[t]} p_{\mathbf{w}}(s) &= \frac{\partial p_{\mathbf{w}}}{\partial y_{\mathbf{w}_2}} \cdot \frac{\partial y_{\mathbf{w}_2}}{\partial z_{\mathbf{w}_2}} \cdot \frac{\partial z_{\mathbf{w}_2}}{\partial y_{\mathbf{w}_1}} \cdot \frac{\partial y_{\mathbf{w}_1}}{\partial z_{\mathbf{w}_1}} \cdot \frac{\partial z_{\mathbf{w}_1}}{\partial s[t]} \\ &= \frac{1}{T} \cdot \frac{\mathbf{w}_2}{1 + (\pi \cdot \mathbf{w}_2 \cdot \Theta(\mathbf{w}_1 \cdot s[t]))^2} \cdot \frac{\mathbf{w}_1}{1 + (\pi \cdot \mathbf{w}_1 \cdot s[t])^2}, \end{aligned}$$

and the cumulative model Jacobian $\nabla_{\mathbf{w}_l} p_{\mathbf{w}}(s)$ of \mathbf{w}_l at each layer l is:

$$\begin{aligned} \nabla_{\mathbf{w}_2} p_{\mathbf{w}}(s) &= \frac{\partial p_{\mathbf{w}}}{\partial y_{\mathbf{w}_2}} \cdot \frac{\partial y_{\mathbf{w}_2}}{\partial z_{\mathbf{w}_2}} \cdot \frac{\partial z_{\mathbf{w}_2}}{\partial \mathbf{w}_2} = \mathbb{E}_T \left[\frac{\Theta(\mathbf{w}_1 \cdot s[t])}{1 + (\pi \cdot \mathbf{w}_2 \cdot \Theta(\mathbf{w}_1 \cdot s[t]))^2} \right] \\ \nabla_{\mathbf{w}_1} p_{\mathbf{w}}(s) &= \frac{\partial p_{\mathbf{w}}}{\partial y_{\mathbf{w}_2}} \cdot \frac{\partial y_{\mathbf{w}_2}}{\partial z_{\mathbf{w}_2}} \cdot \frac{\partial z_{\mathbf{w}_2}}{\partial y_{\mathbf{w}_1}} \cdot \frac{\partial y_{\mathbf{w}_1}}{\partial z_{\mathbf{w}_1}} \cdot \frac{\partial z_{\mathbf{w}_1}}{\partial \mathbf{w}_1} \\ &= \mathbb{E}_T \left[\frac{\mathbf{w}_2}{1 + (\pi \cdot \mathbf{w}_2 \cdot \Theta(\mathbf{w}_1 \cdot s[t]))^2} \cdot \frac{s[t]}{1 + (\pi \cdot \mathbf{w}_1 \cdot s[t])^2} \right] \end{aligned} \quad (10)$$

As obtained from the derivation results, input gradient $\nabla_{s[t]} p_{\mathbf{w}}(s)$ shared a gradient chain $\frac{\partial p_{\mathbf{w}}}{\partial y_{\mathbf{w}_2}} \cdot \frac{\partial y_{\mathbf{w}_2}}{\partial z_{\mathbf{w}_2}} \cdot \frac{\partial z_{\mathbf{w}_2}}{\partial y_{\mathbf{w}_1}} \cdot \frac{\partial y_{\mathbf{w}_1}}{\partial z_{\mathbf{w}_1}}$ with the Jacobian $\nabla_{\mathbf{w}_1} p_{\mathbf{w}}(s)$ of \mathbf{w}_1 during backward computation and a shorter chain of $\frac{\partial p_{\mathbf{w}}}{\partial y_{\mathbf{w}_2}} \cdot \frac{\partial y_{\mathbf{w}_2}}{\partial z_{\mathbf{w}_2}}$ with respect to \mathbf{w}_2 , leading us to the initial observations.¹ \square

We are confident that any sparsity in the shared gradient path propagates backward to both the weight and input gradients. Still, opposite of sparsity, how can we formally quantify the relationship between the density of the weight gradient (specifically of \mathbf{w}_1 , as it is being the closest parameter to input and is highly affected by the shared gradient trail) with respect to input gradient, particularly in the context of Theorem 4.3? To address this, we establish the following theorem, which provides a precise characterization of their relationship:

Theorem 4.4. *Given the same condition as Theorem 4.3, the parameter matrix $\mathbf{w}_l \in \mathbb{R}^{d_1 \times d_2}$ at layer l is said to have a row/column density degree of $k_{\mathbf{w}_l}^{(i)}/k_{\mathbf{w}_l}^{(j)}$ (or $k_{\mathbf{w}_l}^{(i)}/k_{\mathbf{w}_l}^{(j)}$ -dense row/column for short) if each of its row/column vector $\mathbf{w}_l^{(i)}/\mathbf{w}_l^{(j)}$ (where $i \in d_1, j \in d_2$) has at most k non-zero entries $\mathbf{w}_l^{(ij)}$, defined as:*

$$\begin{aligned} k_{\mathbf{w}_l}^{(i)} &= \sup_{i \in d_1} \left(\#\{ \mathbf{w}_l^{(ij)} \in \mathbf{w}_l^{(i)} \mid \mathbf{w}_l^{(ij)} \neq 0 \} \right) = \sup_{i \in d_1} \left(\#\text{supp}(\mathbf{w}_l^{(i)}) \right) = \sup_{i \in d_1} \left(\|\mathbf{w}_l^{(i)}\|_0 \right), \\ k_{\mathbf{w}_l}^{(j)} &= \sup_{j \in d_2} \left(\#\{ \mathbf{w}_l^{(ij)} \in \mathbf{w}_l^{(j)} \mid \mathbf{w}_l^{(ij)} \neq 0 \} \right) = \sup_{j \in d_2} \left(\#\text{supp}(\mathbf{w}_l^{(j)}) \right) = \sup_{j \in d_2} \left(\|\mathbf{w}_l^{(j)}\|_0 \right), \end{aligned} \quad (11)$$

¹A more illustrative demonstration can be found at Figure 6

and for a vector $\mathbf{v} \in \mathbb{R}^d$ as:

$$k_{\mathbf{v}} = \sup_{i \in d} \left(\#\{ \mathbf{v}^{(i)} \in \mathbf{v} | \mathbf{v}^{(i)} \neq 0 \} \right) = \sup_{i \in d} (\#supp(\mathbf{v})) = \sup_{i \in d} (\|\mathbf{v}\|_0). \quad (12)$$

If the L_0 norm of input gradient and weight gradient can be defined as:

$$\begin{aligned} \|\nabla_{s[t]} p_{\mathbf{w}}(s)\|_0 &= \|\mathbf{w}_2 \cdot \mathbf{w}_1\|_0, \\ \|\nabla_{\mathbf{w}_1} p_{\mathbf{w}}(s)\|_0 &= \sum_{t=1}^T \|\mathbf{w}_2 \cdot s[t]\|_0 = \|\mathbf{w}_2 \cdot S\|_0 \quad (S \in \{0,1\}^{d \times T}), \end{aligned} \quad (13)$$

and all weights have $k_{\mathbf{w}_1}^{(i)} > 0, k_{\mathbf{w}_2}^{(j)} > 0$ post optimization, then L_0 norm of weight gradient of \mathbf{w}_1 can be bounded as:

$$\mathbb{E} [\|\nabla_{\mathbf{w}_1} p_{\mathbf{w}}(s)\|_0] \leq \frac{T}{d} \cdot \frac{k_S^{(j)}}{k_{\mathbf{w}_1}^{(j)}} \cdot \mathbb{E} [\|\nabla_{s[t]} p_{\mathbf{w}}(s)\|_0].$$

Proof. Each entry in the input gradient is defined as:

$$\nabla_{s[t]} p_{\mathbf{w}}(s)^{(ij)} = \sum_{n=1}^d \mathbf{w}_2^{(in)} \cdot \mathbf{w}_1^{(nj)} \quad (14)$$

and the probability of an element in the sum chain $\sum_{n=1}^d \mathbf{w}_2^{(in)} \cdot \mathbf{w}_1^{(nj)}$ being dense is upper bounded as:

$$Pr \left(\mathbf{w}_2^{(in)} \cdot \mathbf{w}_1^{(nj)} \neq 0 \right) \leq \frac{k_{\mathbf{w}_2}^{(i)} k_{\mathbf{w}_1}^{(j)}}{d^2}, \quad (15)$$

As long as there is an element in the sum chain is non-zero, the entry of gradient is non-zero. So, from here we can quantify the bound of the probability of input gradient entry $\nabla_{s[t]} p_{\mathbf{w}}(s)^{(ij)}$ being dense as:

$$Pr \left(\nabla_{s[t]} p_{\mathbf{w}}(s)^{(ij)} \neq 0 \right) \leq \frac{k_{\mathbf{w}_2}^{(i)} k_{\mathbf{w}_1}^{(j)}}{d^2}, \quad (16)$$

and the expectation of the input gradient L_0 norm across $d \times d$ matrix is:

$$\mathbb{E} [\|\nabla_{s[t]} p_{\mathbf{w}}(s)\|_0] \leq k_{\mathbf{w}_2}^{(i)} k_{\mathbf{w}_1}^{(j)}. \quad (17)$$

Similar derivation process can be applied to the \mathbf{w}_1 weight gradient and obtain its L_0 expectation. We start with an element of the sum chain $\sum_{n=1}^d \mathbf{w}_2^{(in)} \cdot S^{(nj)}$ as:

$$Pr \left(\mathbf{w}_2^{(in)} \cdot S^{(nj)} \neq 0 \right) \leq \frac{k_{\mathbf{w}_2}^{(i)} k_S^{(j)}}{d^2}, \quad \Leftrightarrow \quad \mathbb{E} [\|\nabla_{\mathbf{w}_1} p_{\mathbf{w}}(s)\|_0] \leq T \cdot \frac{k_{\mathbf{w}_2}^{(i)} k_S^{(j)}}{d}. \quad (18)$$

Divide obtained inequalities from Equation 17 and 18:

$$\begin{aligned} \frac{\mathbb{E} [\|\nabla_{\mathbf{w}_1} p_{\mathbf{w}}(s)\|_0]}{\mathbb{E} [\|\nabla_{s[t]} p_{\mathbf{w}}(s)\|_0]} &\leq \frac{T \cdot \frac{k_{\mathbf{w}_2}^{(i)} k_S^{(j)}}{d}}{k_{\mathbf{w}_2}^{(i)} k_{\mathbf{w}_1}^{(j)}}, \\ \Leftrightarrow \quad \mathbb{E} [\|\nabla_{\mathbf{w}_1} p_{\mathbf{w}}(s)\|_0] &\leq \frac{T}{d} \cdot \frac{k_{\mathbf{w}_2}^{(i)} k_S^{(j)}}{k_{\mathbf{w}_2}^{(i)} k_{\mathbf{w}_1}^{(j)}} \cdot \mathbb{E} [\|\nabla_{s[t]} p_{\mathbf{w}}(s)\|_0], \\ \Leftrightarrow \quad \mathbb{E} [\|\nabla_{\mathbf{w}_1} p_{\mathbf{w}}(s)\|_0] &\leq \frac{T}{d} \cdot \frac{k_S^{(j)}}{k_{\mathbf{w}_1}^{(j)}} \cdot \mathbb{E} [\|\nabla_{s[t]} p_{\mathbf{w}}(s)\|_0]. \end{aligned} \quad (19)$$

As observed from derivation results, weight gradient density is bounded by input gradient density by a factor of $\frac{T}{d} \cdot \frac{k_S^{(j)}}{k_{\mathbf{w}_1}^{(j)}}$. \square

Combining this with observation from Liu et al. (2024), we can see that there is a clear and chained connection between weight gradient, input gradient and robustness. Any attempt to regularize L_0 norm of input gradient to improve robustness as in Liu et al. (2024) will also dampen magnitude of weight gradient.

5 LIMITATIONS AND FUTURE WORKS

While our study presents strong evidence linking gradient density-sparsity to adversarial robustness-generalization trade off in SNNs, an all-rounded method for proper generalization-adversarial robustness improvement was not proposed. Exploration with respect to traditional adversarial vulnerability benchmarking such as Backward Pass Differentiable Approximation (BPDA) (Athalye et al., 2018a) and Expectation Over Transformation (EOT) attacks (Athalye et al., 2018b) was also not unaddressed.

Still, this lead to several open avenues for exploration such as sparsity-aware architecture design where future architectures could be explicitly designed to balance natural and architectural sparsity, creating an optimal trade-offs between robustness and accuracy. This may involve hybrid pooling mechanisms or novel spike-based normalization layers that retain desirable sparsity characteristics. Optionally, we can also focus on a more effective attack methods on SNN models, targeting those with very sparse gradient causing white-box gradient based attacks to be ineffective.

6 CONCLUSION

In this work, we systematically evaluated the trade off between adversarial robustness and generalization of undefended SNNs. Through benchmarking various datasets, we observed that these models demonstrate competitive robustness against traditional white-box attacks, often surpassing existing SOTA defense mechanisms without any explicit adversarial training or defense augmentation. To investigate the root cause of this behavior, we empirically validated this relationship by analyzing the input gradient distributions of SNN, revealing substantial gradient sparsity across various operations. We further categorized this sparsity into *architectural sparsity*, arising from structural components and *natural sparsity*, which is intrinsic to the spiking nature of SNNs. Our experiments led to a measurable reduction in gradient sparsity and a corresponding decrease in adversarial robustness, while theoretical analysis confirming the trade-off between robustness and generalization.

ACKNOWLEDGMENT

We acknowledge and sincerely thankful for the usage of AI (which is Chat-GPT (OpenAI et al., 2023) in our case) for sentence rephrasing and grammar check within our research.

DATA AVAILABILITY

Source code is publicly available at <https://github.com/luutn2002/grad-obf-snn> (alternatively at Zenodo with DOI 10.5281/zenodo.17581571). CIFAR10 and CIFAR100 dataset is available publicly at <https://www.cs.toronto.edu/~kriz/cifar.html>, CIFAR10-DVS can be found at https://figshare.com/articles/dataset/CIFAR10-DVS_New/4724671.

REFERENCES

Alex, K. (2009). Learning multiple layers of features from tiny images. <https://www.cs.toronto.edu/~kriz/learning-features-2009-TR.pdf>.

Athalye, A., Carlini, N., and Wagner, D. (2018a). Obfuscated gradients give a false sense of security: Circumventing defenses to adversarial examples. In *International conference on machine learning*, pages 274–283. PMLR.

Athalye, A., Engstrom, L., Ilyas, A., and Kwok, K. (2018b). Synthesizing robust adversarial examples. In *International conference on machine learning*, pages 284–293. PMLR.

Auge, D., Hille, J., Mueller, E., and Knoll, A. (2021). A survey of encoding techniques for signal processing in spiking neural networks. *Neural Processing Letters*, 53(6):4693–4710.

Baehrens, D., Schroeter, T., Harmeling, S., Kawanabe, M., Hansen, K., and Müller, K.-R. (2010). How to explain individual classification decisions. *The Journal of Machine Learning Research*, 11:1803–1831.

Blouw, P., Choo, X., Hunsberger, E., and Eliasmith, C. (2019). Benchmarking keyword spotting efficiency on neuromorphic hardware. In *Proceedings of the 7th annual neuro-inspired computational elements workshop*, pages 1–8.

Bu, T., Ding, J., Hao, Z., and Yu, Z. (2023). Rate gradient approximation attack threats deep spiking neural networks. In *Proceedings of the IEEE/CVF Conference on Computer Vision and Pattern Recognition*, pages 7896–7906.

Caruana, R., Lou, Y., Gehrke, J., Koch, P., Sturm, M., and Elhadad, N. (2015). Intelligible models for healthcare: Predicting pneumonia risk and hospital 30-day readmission. In *Proceedings of the 21th ACM SIGKDD International Conference on Knowledge Discovery and Data Mining*, KDD ’15, page 1721–1730, New York, NY, USA. Association for Computing Machinery.

Ding, J., Bu, T., Yu, Z., Huang, T., and Liu, J. (2022). Snn-rat: Robustness-enhanced spiking neural network through regularized adversarial training. *Advances in Neural Information Processing Systems*, 35:24780–24793.

Eshraghian, J. K., Ward, M., Neftci, E. O., Wang, X., Lenz, G., Dwivedi, G., Bennamoun, M., Jeong, D. S., and Lu, W. D. (2023). Training spiking neural networks using lessons from deep learning. *Proceedings of the IEEE*.

Esser, S. K., Appuswamy, R., Merolla, P., Arthur, J. V., and Modha, D. S. (2015). Backpropagation for energy-efficient neuromorphic computing. *Advances in neural information processing systems*, 28.

Fang, W., Chen, Y., Ding, J., Yu, Z., Masquelier, T., Chen, D., Huang, L., Zhou, H., Li, G., and Tian, Y. (2023). Spikingjelly: An open-source machine learning infrastructure platform for spike-based intelligence. *Science Advances*, 9(40):eadi1480.

Fang, W., Yu, Z., Chen, Y., Huang, T., Masquelier, T., and Tian, Y. (2021a). Deep residual learning in spiking neural networks. *Advances in Neural Information Processing Systems*, 34:21056–21069.

Fang, W., Yu, Z., Chen, Y., Masquelier, T., Huang, T., and Tian, Y. (2021b). Incorporating learnable membrane time constant to enhance learning of spiking neural networks. In *Proceedings of the IEEE/CVF international conference on computer vision*, pages 2661–2671.

Flores, A. W., Bechtel, K., and Lowenkamp, C. T. (2016). False positives, false negatives, and false analyses: A rejoinder to machine bias: There’s software used across the country to predict future criminals. and it’s biased against blacks. *Fed. Probation*, 80:38.

Gerstner, W. and Kistler, W. M. (2002). *Spiking neuron models: Single neurons, populations, plasticity*. Cambridge university press.

Goodfellow, I. J., Shlens, J., and Szegedy, C. (2014). Explaining and harnessing adversarial examples. *arXiv preprint arXiv:1412.6572*.

Hu, Y., Tang, H., and Pan, G. (2021). Spiking deep residual networks. *IEEE Transactions on Neural Networks and Learning Systems*, 34(8):5200–5205.

Kim, J., Kim, H., Huh, S., Lee, J., and Choi, K. (2018). Deep neural networks with weighted spikes. *Neurocomputing*, 311:373–386.

Kingma, D. P. and Ba, J. (2014). Adam: A method for stochastic optimization. *arXiv preprint arXiv:1412.6980*.

Kundu, S., Pedram, M., and Beerel, P. A. (2021). Hire-snn: Harnessing the inherent robustness of energy-efficient deep spiking neural networks by training with crafted input noise. In *Proceedings of the IEEE/CVF international conference on computer vision*, pages 5209–5218.

Kurakin, A., Goodfellow, I., and Bengio, S. (2016). Adversarial machine learning at scale. *arXiv preprint arXiv:1611.01236*.

Kurakin, A., Goodfellow, I. J., and Bengio, S. (2018). Adversarial examples in the physical world. In *Artificial intelligence safety and security*, pages 99–112. Chapman and Hall/CRC.

Lee, C., Panda, P., Srinivasan, G., and Roy, K. (2018). Training deep spiking convolutional neural networks with stdp-based unsupervised pre-training followed by supervised fine-tuning. *Frontiers in neuroscience*, 12:435.

Lee, C., Sarwar, S. S., Panda, P., Srinivasan, G., and Roy, K. (2020). Enabling spike-based backpropagation for training deep neural network architectures. *Frontiers in neuroscience*, 14:497482.

Li, H., Liu, H., Ji, X., Li, G., and Shi, L. (2017). Cifar10-dvs: an event-stream dataset for object classification. *Frontiers in neuroscience*, 11:244131.

Liang, L., Hu, X., Deng, L., Wu, Y., Li, G., Ding, Y., Li, P., and Xie, Y. (2021). Exploring adversarial attack in spiking neural networks with spike-compatible gradient. *IEEE transactions on neural networks*

and learning systems, 34(5):2569–2583.

Lin, X., Dong, C., and Liu, X. (2022a). Sfta: spiking neural networks vulnerable to spiking feature transferable attack. In *2022 IEEE 21st International Conference on Ubiquitous Computing and Communications (IUCC/CIT/DSCI/SmartCNS)*, pages 140–149. IEEE.

Lin, X., Dong, C., Liu, X., and Zhang, Y. (2022b). Spa: An efficient adversarial attack on spiking neural networks using spike probabilistic. In *2022 22nd IEEE International Symposium on Cluster, Cloud and Internet Computing (CCGrid)*, pages 366–375. IEEE.

Liu, F., Zhao, W., Chen, Y., Wang, Z., Yang, T., and Jiang, L. (2021). Sstdp: Supervised spike timing dependent plasticity for efficient spiking neural network training. *Frontiers in Neuroscience*, 15:756876.

Liu, Y., Bu, T., Ding, J., Hao, Z., Huang, T., and Yu, Z. (2024). Enhancing adversarial robustness in snns with sparse gradients. *arXiv preprint arXiv:2405.20355*.

Luu, N., Luu, D., Nam, P. N., and Thang, T. C. (2024a). Improvement of spiking neural network with bit plane coding. In *2024 IEEE 16th International Conference on Computational Intelligence and Communication Networks (CICN)*. IEEE.

Luu, N. T., Luu, D. T., Nam, P. N., and Thang, T. C. (2025). Hybrid layer-wise ann-snn with surrogate spike encoding-decoding structure. *arXiv preprint arXiv:2509.24411*.

Luu, N. T., Luu, D. T., Pham, N. N., and Truong, T. C. (2024b). Improvement of spiking neural network with bit planes and color models. *arXiv preprint arXiv:2410.08229*.

Luu, N. T., Onuoha, C., and Thang, T. C. (2023). Blind image quality assessment with multimodal prompt learning. In *2023 IEEE 15th International Conference on Computational Intelligence and Communication Networks (CICN)*, pages 614–618. IEEE.

Luu, N. T., Truong, T. C., and Luu, D. T. (2024c). Universal quantum tomography with deep neural networks. *arXiv preprint arXiv:2407.01734*.

Maass, W. (1997). Networks of spiking neurons: the third generation of neural network models. *Neural networks*, 10(9):1659–1671.

Madry, A., Makelov, A., Schmidt, L., Tsipras, D., and Vladu, A. (2017). Towards deep learning models resistant to adversarial attacks. *arXiv preprint arXiv:1706.06083*.

Marchisio, A., Nanfa, G., Khalid, F., Hanif, M. A., Martina, M., and Shafique, M. (2020). Is spiking secure? a comparative study on the security vulnerabilities of spiking and deep neural networks. In *2020 International joint conference on neural networks (IJCNN)*, pages 1–8. IEEE.

Merolla, P. A., Arthur, J. V., Alvarez-Icaza, R., Cassidy, A. S., Sawada, J., Akopyan, F., Jackson, B. L., Imam, N., Guo, C., Nakamura, Y., Brezzo, B., Vo, I., Esser, S. K., Appuswamy, R., Taba, B., Amir, A., Flickner, M. D., Risk, W. P., Manohar, R., and Modha, D. S. (2014). A million spiking-neuron integrated circuit with a scalable communication network and interface. *Science*, 345(6197):668–673.

Neftci, E. O., Mostafa, H., and Zenke, F. (2019). Surrogate gradient learning in spiking neural networks: Bringing the power of gradient-based optimization to spiking neural networks. *IEEE Signal Processing Magazine*, 36(6):51–63.

Nguyen, D.-A., Tran, X.-T., and Iacopi, F. (2021). A review of algorithms and hardware implementations for spiking neural networks. *Journal of Low Power Electronics and Applications*, 11(2):23.

Nunes, J. D., Carvalho, M., Carneiro, D., and Cardoso, J. S. (2022). Spiking neural networks: A survey. *IEEE Access*, 10:60738–60764.

OpenAI, Achiam, J., Adler, S., Agarwal, S., Ahmad, L., Akkaya, I., Aleman, F. L., Almeida, D., Altenschmidt, J., Altman, S., Anadkat, S., Avila, R., Babuschkin, I., Balaji, S., Balcom, V., Baltescu, P., Bao, H., Bavarian, M., Belgum, J., Bello, I., Berdine, J., Bernadett-Shapiro, G., Berner, C., Bogdonoff, L., Boiko, O., Boyd, M., Brakman, A.-L., Brockman, G., Brooks, T., Brundage, M., Button, K., Cai, T., Campbell, R., Cann, A., Carey, B., Carlson, C., Carmichael, R., Chan, B., Chang, C., Chantzis, F., Chen, D., Chen, S., Chen, R., Chen, J., Chen, M., Chess, B., Cho, C., Chu, C., Chung, H. W., Cummings, D., Currier, J., Dai, Y., Decareaux, C., Degry, T., Deutsch, N., Deville, D., Dhar, A., Dohan, D., Dowling, S., Dunning, S., Ecoffet, A., Eleti, A., Eloundou, T., Farhi, D., Fedus, L., Felix, N., Fishman, S. P., Forte, J., Fulford, I., Gao, L., Georges, E., Gibson, C., Goel, V., Gogineni, T., Goh, G., Gontijo-Lopes, R., Gordon, J., Grafstein, M., Gray, S., Greene, R., Gross, J., Gu, S. S., Guo, Y., Hallacy, C., Han, J., Harris, J., He, Y., Heaton, M., Heidecke, J., Hesse, C., Hickey, A., Hickey, W., Hoeschele, P., Houghton, B., Hsu, K., Hu, S., Hu, X., Huizinga, J., Jain, S., Jain, S., Jang, J., Jiang, A., Jiang, R., Jin, H., Jin, D., Jomoto, S., Jonn, B., Jun, H., Kaftan, T., Łukasz Kaiser, Kamali, A., Kanitscheider, I., Keskar, N. S., Khan, T., Kilpatrick, L., Kim, J. W., Kim, C., Kim, Y., Kirchner, J. H., Kiros, J., Knight, M., Kokotajlo,

D., Łukasz Kondraciuk, Kondrich, A., Konstantinidis, A., Kosic, K., Krueger, G., Kuo, V., Lampe, M., Lan, I., Lee, T., Leike, J., Leung, J., Levy, D., Li, C. M., Lim, R., Lin, M., Lin, S., Litwin, M., Lopez, T., Lowe, R., Lue, P., Makanju, A., Malfacini, K., Manning, S., Markov, T., Markovski, Y., Martin, B., Mayer, K., Mayne, A., McGrew, B., McKinney, S. M., McLeavey, C., McMillan, P., McNeil, J., Medina, D., Mehta, A., Menick, J., Metz, L., Mishchenko, A., Mishkin, P., Monaco, V., Morikawa, E., Mossing, D., Mu, T., Murati, M., Murk, O., Mély, D., Nair, A., Nakano, R., Nayak, R., Neelakantan, A., Ngo, R., Noh, H., Ouyang, L., O’Keefe, C., Pachocki, J., Paino, A., Palermo, J., Pantuliano, A., Parascandolo, G., Parish, J., Parparita, E., Passos, A., Pavlov, M., Peng, A., Perelman, A., de Avila Belbute Peres, F., Petrov, M., de Oliveira Pinto, H. P., Michael, Pokorny, Pokrass, M., Pong, V. H., Powell, T., Power, A., Power, B., Proehl, E., Puri, R., Radford, A., Rae, J., Ramesh, A., Raymond, C., Real, F., Rimbach, K., Ross, C., Rotsted, B., Roussez, H., Ryder, N., Saltarelli, M., Sanders, T., Santurkar, S., Sastry, G., Schmidt, H., Schnurr, D., Schulman, J., Selsam, D., Sheppard, K., Sherbakov, T., Shieh, J., Shoker, S., Shyam, P., Sidor, S., Sigler, E., Simens, M., Sitkin, J., Slama, K., Sohl, I., Sokolowsky, B., Song, Y., Staudacher, N., Such, F. P., Summers, N., Sutskever, I., Tang, J., Tezak, N., Thompson, M. B., Tillet, P., Tootoonchian, A., Tseng, E., Tuggle, P., Turley, N., Tworek, J., Uribe, J. F. C., Vallone, A., Vijayvergiya, A., Voss, C., Wainwright, C., Wang, J. J., Wang, A., Wang, B., Ward, J., Wei, J., Weinmann, C., Welihinda, A., Welinder, P., Weng, J., Weng, L., Wiethoff, M., Willner, D., Winter, C., Wolrich, S., Wong, H., Workman, L., Wu, S., Wu, J., Wu, M., Xiao, K., Xu, T., Yoo, S., Yu, K., Yuan, Q., Zaremba, W., Zellers, R., Zhang, C., Zhang, M., Zhao, S., Zheng, T., Zhuang, J., Zhuk, W., and Zoph, B. (2023). Gpt-4 technical report. *arXiv preprint arXiv:2303.08774*.

Papernot, N., McDaniel, P., Goodfellow, I., Jha, S., Celik, Z. B., and Swami, A. (2017). Practical black-box attacks against machine learning. In *Proceedings of the 2017 ACM on Asia conference on computer and communications security*, pages 506–519.

Paszke, A., Gross, S., Massa, F., Lerer, A., Bradbury, J., Chanan, G., Killeen, T., Lin, Z., Gimelshein, N., Antiga, L., Desmaison, A., Kopf, A., Yang, E., DeVito, Z., Raison, M., Tejani, A., Chilamkurthy, S., Steiner, B., Fang, L., Bai, J., and Chintala, S. (2019). Pytorch: An imperative style, high-performance deep learning library. *Advances in neural information processing systems*, 32.

Picard, D. (2021). Torch. manual_seed (3407) is all you need: On the influence of random seeds in deep learning architectures for computer vision. *arXiv preprint arXiv:2109.08203*.

Rajendran, B., Sebastian, A., Schmuker, M., Srinivasa, N., and Eleftheriou, E. (2019). Low-power neuromorphic hardware for signal processing applications: A review of architectural and system-level design approaches. *IEEE Signal Processing Magazine*, 36(6):97–110.

Ribeiro, M. T., Singh, S., and Guestrin, C. (2016). ” why should i trust you?” explaining the predictions of any classifier. In *Proceedings of the 22nd ACM SIGKDD international conference on knowledge discovery and data mining*, pages 1135–1144.

Ross, A. and Doshi-Velez, F. (2018). Improving the adversarial robustness and interpretability of deep neural networks by regularizing their input gradients. In *Proceedings of the AAAI conference on artificial intelligence*, volume 32.

Ross, A. S., Hughes, M. C., and Doshi-Velez, F. (2017). Right for the right reasons: Training differentiable models by constraining their explanations. *arXiv preprint arXiv:1703.03717*.

Rueckauer, B., Lungu, I.-A., Hu, Y., Pfeiffer, M., and Liu, S.-C. (2017). Conversion of continuous-valued deep networks to efficient event-driven networks for image classification. *Frontiers in neuroscience*, 11:682.

Rumelhart, D. E., Hinton, G. E., and Williams, R. J. (1986). Learning representations by back-propagating errors. *nature*, 323(6088):533–536.

Shalev-Shwartz, S., Shamir, O., and Shammah, S. (2017). Failures of gradient-based deep learning. In *International Conference on Machine Learning*, pages 3067–3075. PMLR.

Sharmin, S., Panda, P., Sarwar, S. S., Lee, C., Ponghiran, W., and Roy, K. (2019). A comprehensive analysis on adversarial robustness of spiking neural networks. In *2019 International Joint Conference on Neural Networks (IJCNN)*, pages 1–8. IEEE.

Sharmin, S., Rathi, N., Panda, P., and Roy, K. (2020). Inherent adversarial robustness of deep spiking neural networks: Effects of discrete input encoding and non-linear activations. In *European Conference on Computer Vision*, pages 399–414. Springer.

Shrestha, S. B. and Orchard, G. (2018). Slayer: Spike layer error reassignment in time. *Advances in neural information processing systems*, 31.

Smilkov, D., Thorat, N., Kim, B., Viégas, F., and Wattenberg, M. (2017). Smoothgrad: removing noise by adding noise. *arXiv preprint arXiv:1706.03825*.

Srinivasan, G., Roy, S., Raghunathan, V., and Roy, K. (2017). Spike timing dependent plasticity based enhanced self-learning for efficient pattern recognition in spiking neural networks. In *2017 International Joint Conference on Neural Networks (IJCNN)*, pages 1847–1854. IEEE.

Sundararajan, M., Taly, A., and Yan, Q. (2016). Gradients of counterfactuals. *arXiv preprint arXiv:1611.02639*.

Szegedy, C., Zaremba, W., Sutskever, I., Bruna, J., Erhan, D., Goodfellow, I., and Fergus, R. (2013). Intriguing properties of neural networks. *arXiv preprint arXiv:1312.6199*.

Tramèr, F., Kurakin, A., Papernot, N., Goodfellow, I., Boneh, D., and McDaniel, P. (2017a). Ensemble adversarial training: Attacks and defenses. *arXiv preprint arXiv:1705.07204*.

Tramèr, F., Papernot, N., Goodfellow, I., Boneh, D., and McDaniel, P. (2017b). The space of transferable adversarial examples. *arXiv preprint arXiv:1704.03453*.

Tsipras, D., Santurkar, S., Engstrom, L., Turner, A., and Madry, A. (2018). Robustness may be at odds with accuracy. *arXiv preprint arXiv:1805.12152*.

Wang, J. and Perez, L. (2017). The effectiveness of data augmentation in image classification using deep learning. *Convolutional Neural Networks Vis. Recognit*, 11(2017):1–8.

Wani, M. A., Bhat, F. A., Afzal, S., and Khan, A. I. (2020). *Advances in deep learning*. Springer.

Xu, W., Evans, D., and Qi, Y. (2017). Feature squeezing: Detecting adversarial examples in deep neural networks. *arXiv preprint arXiv:1704.01155*.

Zakon, E. (2004). Mathematical analysis. volume i/zakon, elias. *West Lafayette, Indiana, USA*.

Zenke, F. and Ganguli, S. (2018). Superspike: Supervised learning in multilayer spiking neural networks. *Neural computation*, 30(6):1514–1541.

Zenke, F. and Vogels, T. P. (2021). The remarkable robustness of surrogate gradient learning for instilling complex function in spiking neural networks. *Neural computation*, 33(4):899–925.

A PROOF FOR GRADIENT DENSITY-ADVERSARIAL VULNERABILITY RELATIONSHIP

As priorly addressed by Liu et al. (2024), we first define some definition:

Definition A.1 (Random Vulnerability). *The random vulnerability of f at point x to an ℓ_p attack of size ϵ is defined as the expected value of $(f_y(x + \epsilon \cdot \delta) - f_y(x))^2$, where δ follows a uniform distribution \mathcal{U} within the unit ℓ_p ball, and y denotes the class of x . Mathematically, it can be expressed as:*

$$\rho_{\text{rand}}(f, x, \epsilon, \ell_p) = \mathbb{E}_{\delta \sim \mathcal{U}(\{\|\delta\|_p \leq 1\})} (f_y(x + \epsilon \cdot \delta) - f_y(x))^2. \quad (20)$$

Definition A.2 (Adversarial Vulnerability). *The adversarial vulnerability of f at point x to an ℓ_p attack of size ϵ is defined as the supremum of $(f_y(x + \epsilon \cdot \delta) - f_y(x))^2$, where δ follows a uniform distribution \mathcal{U} within the unit ℓ_p ball, and y denotes the class of x . Mathematically, it can be expressed as:*

$$\rho_{\text{adv}}(f, x, \epsilon, \ell_p) = \sup_{\delta \sim \mathcal{U}(\{\|\delta\|_p \leq 1\})} (f_y(x + \epsilon \cdot \delta) - f_y(x))^2. \quad (21)$$

We want to prove that:

Theorem A.1 (Liu et al.). *Suppose f is a differentiable SNN by surrogate gradients, and ϵ is the magnitude of an attack, assumed to be small enough. Given an input image \mathbf{x} with corresponding label y , the ratio of adversarial vulnerability $\rho_{\text{adv}}(f, \mathbf{x}, \epsilon, \ell_\infty)$ and random vulnerability $\rho_{\text{rand}}(f, \mathbf{x}, \epsilon, \ell_\infty)$ is upper bounded by the density of input gradient $\nabla_{\mathbf{x}} f_y$ as:*

$$3 \leq \frac{\rho_{\text{adv}}(f, \mathbf{x}, \epsilon, \ell_\infty)}{\rho_{\text{rand}}(f, \mathbf{x}, \epsilon, \ell_\infty)} \leq 3 \|\nabla_{\mathbf{x}} f_y(\mathbf{x})\|_0. \quad (22)$$

where $\rho_{\text{adv}}(f, \mathbf{x}, \epsilon, \ell_\infty)$ scale linearly with non-zeros entries (L_0 norm) of input gradient $\|\nabla_{\mathbf{x}} f_y(\mathbf{x})\|_0$.

Proof. Let us assume that f is differentiable, and that a surrogate gradient is employed for backpropagation. For sufficiently small ϵ , we can apply the first-order Taylor expansion of $f_y(x + \epsilon \cdot \delta)$ around $f_y(x)$:

$$f_y(x + \epsilon \cdot \delta) \approx f_y(x) + \epsilon \nabla f_y(x)^\top \delta. \quad (23)$$

Consequently,

$$f_y(x + \epsilon \cdot \delta) - f_y(x) \approx \epsilon \nabla f_y(x)^\top \delta. \quad (24)$$

When $\delta \in \mathbb{R}^m$ and each component δ_i follows uniform distribution $\mathcal{U}(-1, 1)$, the expectation of their pairwise product is given by

$$\mathbb{E}[\delta_i \delta_j] = \begin{cases} 0, & i \neq j, \\ \frac{1}{3}, & i = j. \end{cases} \quad (25)$$

Thus, the random perturbation measure $\rho_{\text{rand}}(f, x, \epsilon, \ell_\infty)$ can be approximated as

$$\begin{aligned} \rho_{\text{rand}}(f, x, \epsilon, \ell_\infty) &= \mathbb{E}_{\delta \sim \text{Unif}(\text{cube})} \left[(f_y(x + \epsilon \cdot \delta) - f_y(x))^2 \right] \\ &\approx \epsilon^2 \nabla f_y(x)^\top \mathbb{E}_\delta [\delta \delta^\top] \nabla f_y(x) \\ &= \frac{1}{3} \epsilon^2 \|\nabla f_y(x)\|_2^2. \end{aligned} \quad (26)$$

Similarly, the adversarial perturbation measure is approximated by

$$\begin{aligned} \rho_{\text{adv}}(f, x, \epsilon, \ell_\infty) &= \sup_{\delta \sim \text{Unif}(\text{cube})} (f_y(x + \epsilon \cdot \delta) - f_y(x))^2 \\ &\approx \epsilon^2 \sup_{\delta} \left| \nabla f_y(x)^\top \delta \right|^2 \\ &= \epsilon^2 \left(\nabla f_y(x)^\top \text{sign}(\nabla f_y(x)) \right)^2 \\ &= \epsilon^2 \|\nabla f_y(x)\|_1^2. \end{aligned} \quad (27)$$

The ratio between the adversarial and random perturbation effects is therefore approximated by

$$\frac{\rho_{\text{adv}}(f, x, \epsilon, \ell_\infty)}{\rho_{\text{rand}}(f, x, \epsilon, \ell_\infty)} \approx 3 \frac{\|\nabla f_y(x)\|_1^2}{\|\nabla f_y(x)\|_2^2}. \quad (28)$$

For any $u \in \mathbb{R}^m$, it holds that $\|u\|_1 \geq \|u\|_2$ since

$$\|u\|_1^2 = \left(\sum_{i=1}^m |u_i| \right)^2 = \sum_{i=1}^m u_i^2 + \sum_i \sum_{j \neq i} |u_i u_j| \geq \sum_{i=1}^m u_i^2 = \|u\|_2^2. \quad (29)$$

Furthermore, if $a \in \mathbb{R}^m$ is defined by $a_i = \text{sign}(u_i)$, then by the Cauchy–Schwarz inequality we obtain

$$\begin{aligned} \|u\|_1 &= \sum_{i=1}^m |u_i| = \sum_{i=1}^m u_i a_i \leq \left(\sum_{i=1}^m u_i^2 \right)^{1/2} \left(\sum_{i=1}^m a_i^2 \right)^{1/2} \\ &= \|u\|_2 \sqrt{\|u\|_0}. \end{aligned} \quad (30)$$

which can be bounded as

$$3 \leq \frac{\rho_{\text{adv}}(f, x, \epsilon, \ell_\infty)}{\rho_{\text{rand}}(f, x, \epsilon, \ell_\infty)} \leq 3 \|\nabla f_y(x)\|_0. \quad (31)$$

□

B PROOF FOR TEMPORAL RELATIONSHIP BETWEEN GRADIENT SCALE AND PERFORMANCE

Firstly, we will provide some background knowledge to assist our mathematical derivation. Given a SNN model that employ hard-reset IF neurons with BPTT (Fang et al., 2021a; Eshraghian et al., 2023; Fang et al., 2023; Luu et al., 2025), optimization scheme is defined as:

$$\begin{aligned}
u_i^{(l)}(t) &= (1 - s_i^{(l)}(t-1)) u_i^{(l)}(t-1) + W^{(l)} s^{(l-1)}(t) + b_i^{(l)}, \\
s_i^{(l)}(t) &= \Theta(u_i^{(l)}(t), V_{th}) \\
\Theta(x, V_{th}) &= \begin{cases} 1 & \text{if } x - V_{th} \geq 0 \\ 0 & \text{otherwise} \end{cases} \\
\frac{\partial \mathcal{L}}{\partial W^{(l)}} &= \sum_{t=1}^T \frac{\partial \mathcal{L}}{\partial s^{(l)}(t)} \cdot \frac{\partial s^{(l)}(t)}{\partial u^{(l)}(t)} \cdot \frac{\partial u^{(l)}(t)}{\partial W^{(l)}}
\end{aligned} \tag{32}$$

where:

- $u_i^{(l)}(t)$ is the membrane potential of neuron i in layer l at time $t \in T$,
- $s_i^{(l)}(t)$ is the spike output of neuron i , similarly with prior layer signal $s_i^{(l-1)}(t)$,
- V_{th} is the threshold voltage,
- synaptic weight $W^{(l)}$ and bias $b_i^{(l)}$,
- Θ is the Heaviside function,
- loss function \mathcal{L} and it's gradient with respect to weight $\frac{\partial \mathcal{L}}{\partial W^{(l)}}$.

Signal-to-noise-ratio (SNR) from prior work of Shalev-Shwartz et al. (2017) is adaptable to surrogate SNN model trained via timestep T by substitute results from Equation 32 as:

$$\begin{aligned}
SNR(\delta(\mathbf{x})) &= \frac{\|\mathbb{E}_{\mathbf{x}}[\delta(\mathbf{x})]\|_2^2}{\mathbb{E}_{\mathbf{x}}\|\delta(\mathbf{x}) - \mathbb{E}_{\mathbf{x}}[\delta(\mathbf{x})]\|_2^2}, \\
\delta(\mathbf{x}) &= h(\mathbf{x}) \cdot g_{\mathbf{w}}(\mathbf{x}) \\
&= h(\mathbf{x}) \cdot \sum_{t=1}^T \frac{\partial s^{(l)}(t)}{\partial u^{(l)}(t)} \cdot \frac{\partial u^{(l)}(t)}{\partial W^{(l)}}
\end{aligned} \tag{33}$$

where $g_{\mathbf{w}}(\mathbf{x}) = \frac{\partial}{\partial \mathbf{w}} p_{\mathbf{w}}(\mathbf{x})$ is the Jacobian of model $p_{\mathbf{w}}(\mathbf{x})$ with respect to model weight \mathbf{w} . Under the case of extending over temporal dimension by timestep T_2 , we would have $\delta^{extend}(\mathbf{x})$:

$$\begin{aligned}
\delta^{extend}(\mathbf{x}) &= h(\mathbf{x}) \cdot \left(\sum_{t=1}^T \frac{\partial s^{(l)}(t)}{\partial u^{(l)}(t)} \cdot \frac{\partial u^{(l)}(t)}{\partial W^{(l)}} + \sum_{t=1}^{T_2} \frac{\partial s^{(l)}(t)}{\partial u^{(l)}(t)} \cdot \frac{\partial u^{(l)}(t)}{\partial W^{(l)}} \right) \\
&= h(\mathbf{x}) \cdot g_{\mathbf{w}}(\mathbf{x}) + h(\mathbf{x}) \cdot g_{\mathbf{w}}^{T_2}(\mathbf{x}) \\
&= h(\mathbf{x}) \cdot g_{\mathbf{w}}^{extend}(\mathbf{x})
\end{aligned} \tag{34}$$

Our theorem is stated as follow:

Theorem B.1. Assume that temporally-extended gradient $g_{\mathbf{w}}^{extend}(\mathbf{x})$ does not explode nor vanish, bounded as:

$$G(\mathbf{w})^2 > \left\| \mathbb{E}_{\mathbf{x}}[g_{\mathbf{w}}^{extend}(\mathbf{x})] \right\|_{\infty} > 0$$

for some scalar $G(\mathbf{w})$, where both gradient of baseline SNN $g_{\mathbf{w}}(\mathbf{x})$ and temporally extended SNN $g_{\mathbf{w}}^{extend}(\mathbf{x})$ converge toward a reasonable approximation of $h(\mathbf{x})$ and have similar distribution that satisfy:

$$\text{Cov}\left(h(\mathbf{x}), g_{\mathbf{w}}^{extend}(\mathbf{x})\right) = 0, \quad \text{sign}(\mathbb{E}_{\mathbf{x}}[h(\mathbf{x})]) > 0, \quad h(\mathbf{x}) \cdot g_{\mathbf{w}}^{extend}(\mathbf{x}) \sim h(\mathbf{x}) \cdot g_{\mathbf{w}}(\mathbf{x}),$$

there exist:

$$\sup\left(SNR\left(\delta^{extend}(\mathbf{x})\right)\right) \geq \sup(SNR(\delta(\mathbf{x}))).$$

where:

$$\begin{aligned} \sup\left(SNR(\delta^{extend}(\mathbf{x}))\right) &= \frac{\left\|\mathbb{E}_{\mathbf{x}}\left[\delta^{extend}(\mathbf{x})\right]\right\|_{\infty}^2}{\mathbb{E}_{\mathbf{x}}\left\|\delta^{extend}(\mathbf{x}) - \mathbb{E}_{\mathbf{x}}\left[\delta^{extend}(\mathbf{x})\right]\right\|_{\infty}^2}, \\ \sup(SNR(\delta(\mathbf{x}))) &= \frac{\left\|\mathbb{E}_{\mathbf{x}}[\delta(\mathbf{x})]\right\|_{\infty}^2}{\mathbb{E}_{\mathbf{x}}\left\|\delta(\mathbf{x}) - \mathbb{E}_{\mathbf{x}}[\delta(\mathbf{x})]\right\|_{\infty}^2} \end{aligned}$$

Proof. In order to prove Theorem B.1, we first need some auxiliary lemmas to be proven.

Lemma B.1. Assuming temporally extended SNN model $p_{\mathbf{w}}^{extend}(\mathbf{x})$ reasonably approximate $h(\mathbf{x})$ such that Jacobian of extended SNN $g_{\mathbf{w}}^{extend}(\mathbf{x})$ satisfy:

$$\text{Cov}\left(h(\mathbf{x}), g_{\mathbf{w}}^{extend}(\mathbf{x})\right) = 0, \quad \text{sign}(\mathbb{E}_{\mathbf{x}}[h(\mathbf{x})]) > 0,$$

while extended gradient does not explode nor vanish over stochastic estimation, bounded as:

$$G(\mathbf{w})^2 > \left\|\mathbb{E}_{\mathbf{x}}\left[g_{\mathbf{w}}^{extend}(\mathbf{x})\right]\right\|_{\infty} > 0 \quad (35)$$

for some scalar $G(\mathbf{w})$, there exist:

$$\left\|\mathbb{E}_{\mathbf{x}}\left[\delta^{extend}(\mathbf{x})\right]\right\|_{\infty}^2 \geq \left\|\mathbb{E}_{\mathbf{x}}[\delta(\mathbf{x})]\right\|_{\infty}^2.$$

Proof. In order for the resulted inequality in our lemma exist, we need to prove that under given condition, there exist:

$$\begin{cases} \sup\left(\mathbb{E}_{\mathbf{x}}\left[\delta^{extend}(\mathbf{x})\right]\right) \geq \sup(\mathbb{E}_{\mathbf{x}}[\delta(\mathbf{x})]), \\ \inf\left(\mathbb{E}_{\mathbf{x}}\left[\delta^{extend}(\mathbf{x})\right]\right) \leq \inf(\mathbb{E}_{\mathbf{x}}[\delta(\mathbf{x})]). \end{cases}$$

As noted from initial condition in Equation 35, we have:

$$\begin{aligned} G(\mathbf{w})^2 &> \left\|\mathbb{E}_{\mathbf{x}}\left[g_{\mathbf{w}}^{extend}(\mathbf{x})\right]\right\|_{\infty} > 0 \\ \Leftrightarrow \sup\left(\mathbb{E}_{\mathbf{x}}\left[g_{\mathbf{w}}^{extend}(\mathbf{x})\right]\right) &\geq 0 \\ \Leftrightarrow \sup(\mathbb{E}_{\mathbf{x}}[h(\mathbf{x})]) \cdot \sup\left(\mathbb{E}_{\mathbf{x}}\left[g_{\mathbf{w}}^{extend}(\mathbf{x})\right]\right) &\geq 0 \\ \Leftrightarrow \sup\left(\mathbb{E}_{\mathbf{x}}[h(\mathbf{x})] \cdot \mathbb{E}_{\mathbf{x}}\left[g_{\mathbf{w}}^{extend}(\mathbf{x})\right] + \text{Cov}\left(h(\mathbf{x}), g_{\mathbf{w}}^{extend}(\mathbf{x})\right)\right) &\geq 0 \\ \Leftrightarrow \sup\left(\mathbb{E}_{\mathbf{x}}\left[h(\mathbf{x}) \cdot g_{\mathbf{w}}^{extend}(\mathbf{x})\right]\right) &\geq 0 \\ \Leftrightarrow \sup(\mathbb{E}_{\mathbf{x}}[h(\mathbf{x}) \cdot g_{\mathbf{w}}(\mathbf{x})]) + \sup\left(\mathbb{E}_{\mathbf{x}}\left[h(\mathbf{x}) \cdot g_{\mathbf{w}}^{extend}(\mathbf{x})\right]\right) &\geq \sup(\mathbb{E}_{\mathbf{x}}[h(\mathbf{x}) \cdot g_{\mathbf{w}}(\mathbf{x})]) \end{aligned}$$

Under the property of expectation's sum and Minkowski's sum (Zakon, 2004):

$$\begin{aligned} \Leftrightarrow \sup\left(\mathbb{E}_{\mathbf{x}}\left[h(\mathbf{x}) \cdot g_{\mathbf{w}}^{extend}(\mathbf{x})\right]\right) &\geq \sup(\mathbb{E}_{\mathbf{x}}[h(\mathbf{x}) \cdot g_{\mathbf{w}}(\mathbf{x})]) \\ \Leftrightarrow \sup\left(\mathbb{E}_{\mathbf{x}}\left[\delta^{extend}(\mathbf{x})\right]\right) &\geq \sup(\mathbb{E}_{\mathbf{x}}[\delta(\mathbf{x})]). \end{aligned}$$

We can then use a similar process with infimum inequality of initial condition:

$$\begin{aligned}
G(\mathbf{w})^2 &> \left\| \mathbb{E}_{\mathbf{x}} \left[g_{\mathbf{w}}^{\text{extend}}(\mathbf{x}) \right] \right\|_{\infty}^2 > 0 \\
\Leftrightarrow \inf \left(\mathbb{E}_{\mathbf{x}} \left[g_{\mathbf{w}}^{\text{extend}}(\mathbf{x}) \right] \right) &\leq 0 \\
\Leftrightarrow \inf \left(\mathbb{E}_{\mathbf{x}} [h(\mathbf{x})] \right) \cdot \inf \left(\mathbb{E}_{\mathbf{x}} \left[g_{\mathbf{w}}^{\text{extend}}(\mathbf{x}) \right] \right) &\leq 0 \\
\Leftrightarrow \inf \left(\mathbb{E}_{\mathbf{x}} [h(\mathbf{x})] \cdot \mathbb{E}_{\mathbf{x}} \left[g_{\mathbf{w}}^{\text{extend}}(\mathbf{x}) \right] + \text{Cov} \left(h(\mathbf{x}), g_{\mathbf{w}}^{\text{extend}}(\mathbf{x}) \right) \right) &\leq 0 \\
\Leftrightarrow \inf \left(\mathbb{E}_{\mathbf{x}} \left[h(\mathbf{x}) \cdot g_{\mathbf{w}}^{\text{extend}}(\mathbf{x}) \right] \right) &\leq 0 \\
\Leftrightarrow \inf \left(\mathbb{E}_{\mathbf{x}} [h(\mathbf{x}) \cdot g_{\mathbf{w}}(\mathbf{x})] \right) + \inf \left(\mathbb{E}_{\mathbf{x}} \left[h(\mathbf{x}) \cdot g_{\mathbf{w}}^{\text{extend}}(\mathbf{x}) \right] \right) &\leq \inf \left(\mathbb{E}_{\mathbf{x}} [h(\mathbf{x}) \cdot g_{\mathbf{w}}(\mathbf{x})] \right) \\
\Leftrightarrow \inf \left(\mathbb{E}_{\mathbf{x}} \left[h(\mathbf{x}) \cdot g_{\mathbf{w}}^{\text{extend}}(\mathbf{x}) \right] \right) &\leq \inf \left(\mathbb{E}_{\mathbf{x}} [h(\mathbf{x}) \cdot g_{\mathbf{w}}(\mathbf{x})] \right) \\
\Leftrightarrow \inf \left(\mathbb{E}_{\mathbf{x}} \left[\delta^{\text{extend}}(\mathbf{x}) \right] \right) &\leq \inf \left(\mathbb{E}_{\mathbf{x}} [\delta(\mathbf{x})] \right)
\end{aligned}$$

From here we can conclude that there exist:

$$\left\| \mathbb{E}_{\mathbf{x}} \left[\delta^{\text{extend}}(\mathbf{x}) \right] \right\|_{\infty}^2 \geq \left\| \mathbb{E}_{\mathbf{x}} [\delta(\mathbf{x})] \right\|_{\infty}^2$$

under given condition. \square

Lemma B.2. Assuming both gradient of baseline SNN $g_{\mathbf{w}}(\mathbf{x})$ and extended SNN $g_{\mathbf{w}}^{\text{extend}}(\mathbf{x})$ converge toward a reasonable approximation of $h(\mathbf{x})$ and have similar distribution that satisfy:

$$h(\mathbf{x}) \cdot g_{\mathbf{w}}^{\text{extend}}(\mathbf{x}) \sim h(\mathbf{x}) \cdot g_{\mathbf{w}}(\mathbf{x}),$$

there exist:

$$\mathbb{E}_{\mathbf{x}} \left\| \delta^{\text{extend}}(\mathbf{x}) - \mathbb{E}_{\mathbf{x}} \left[\delta^{\text{extend}}(\mathbf{x}) \right] \right\|_{\infty}^2 = \mathbb{E}_{\mathbf{x}} \left\| \delta(\mathbf{x}) - \mathbb{E}_{\mathbf{x}} [\delta(\mathbf{x})] \right\|_{\infty}^2.$$

Proof. Since we have the initial condition that:

$$h(\mathbf{x}) \cdot g_{\mathbf{w}}^{\text{extend}}(\mathbf{x}) \sim h(\mathbf{x}) \cdot g_{\mathbf{w}}(\mathbf{x}),$$

then:

$$\begin{aligned}
g_{\mathbf{w}}^{\text{extend}}(\mathbf{x}) &\sim g_{\mathbf{w}}(\mathbf{x}) \\
\Leftrightarrow \text{Var} \left(\delta^{\text{extend}}(\mathbf{x}) \right) &= \text{Var} (\delta(\mathbf{x})) \\
\Leftrightarrow \left\| \delta^{\text{extend}}(\mathbf{x}) - \mathbb{E}_{\mathbf{x}} \left[\delta^{\text{extend}}(\mathbf{x}) \right] \right\|_{\infty}^2 &= \left\| \delta(\mathbf{x}) - \mathbb{E}_{\mathbf{x}} [\delta(\mathbf{x})] \right\|_{\infty}^2 \\
\Leftrightarrow \mathbb{E}_{\mathbf{x}} \left\| \delta^{\text{extend}}(\mathbf{x}) - \mathbb{E}_{\mathbf{x}} \left[\delta^{\text{extend}}(\mathbf{x}) \right] \right\|_{\infty}^2 &= \mathbb{E}_{\mathbf{x}} \left\| \delta(\mathbf{x}) - \mathbb{E}_{\mathbf{x}} [\delta(\mathbf{x})] \right\|_{\infty}^2.
\end{aligned} \tag{36}$$

\square

From results of Lemma B.1 and B.2, we can conclude that there exist:

$$\begin{aligned}
\frac{\left\| \mathbb{E}_{\mathbf{x}} \left[\delta^{\text{extend}}(\mathbf{x}) \right] \right\|_{\infty}^2}{\mathbb{E}_{\mathbf{x}} \left\| \delta^{\text{extend}}(\mathbf{x}) - \mathbb{E}_{\mathbf{x}} \left[\delta^{\text{extend}}(\mathbf{x}) \right] \right\|_{\infty}^2} &\geq \frac{\left\| \mathbb{E}_{\mathbf{x}} [\delta(\mathbf{x})] \right\|_{\infty}^2}{\mathbb{E}_{\mathbf{x}} \left\| \delta(\mathbf{x}) - \mathbb{E}_{\mathbf{x}} [\delta(\mathbf{x})] \right\|_{\infty}^2} \\
\Leftrightarrow \sup \left(\text{SNR} \left(\delta^{\text{extend}}(\mathbf{x}) \right) \right) &\geq \sup \left(\text{SNR} (\delta(\mathbf{x})) \right).
\end{aligned}$$

\square